

# Ray travel times in range-dependent acoustic waveguides

Anatoly L. Virovlyansky

*Institute of Applied Physics, Russian Academy of Science,  
46 Ul'yanov Street, 603600 Nizhny Novgorod, Russia*

## Abstract

An approximate analytical approach to describe the stochastic motion of sound rays in deep ocean is developed. This is done for a realistic propagation model with an internal wave induced perturbation imposed on the smooth background sound speed field. The chaotic ray dynamics is analyzed using the Hamiltonian formalism taken in terms of the action-angle canonical variables. It is shown that even at ranges of a few thousands km, the magnitude of range variations of the action variable is still small enough to be used as a small parameter in the problem. A simple expression for the difference in travel times of perturbed and unperturbed rays and approximate analytical solutions to stochastic ray (Hamilton) equations are derived. These relations are applied to study range variations of the timefront (representing ray arrivals in the time-depth plane). Estimations characterizing the widening and bias of timefront segments in the presence of perturbations are obtained. Qualitative and quantitative explanations are given to surprising stability of early portions of timefronts observed in both numerical simulations and field experiments.

## 1 Introduction

We consider the ray dynamics in a deep ocean acoustic waveguide with an internal wave induced perturbation to the smooth (background) sound speed field. It is assumed that statistics of random internal

waves are determined by the empirical Garrett-Munk spectrum [1, 2, 3]. Numerical simulations demonstrate that although this perturbation is weak, it gives rise to a rather strong ray chaos [3, 4]. In the presence of internal waves ray trajectories exhibit extreme sensitivity to initial conditions and at ranges of a few thousand km parameters of a ray trajectory with the given starting depth and launch angle are practically unpredictable and can be described only statistically. On the other hand, even under conditions of ray chaos the arrival pattern retains some of its features observed in the unperturbed waveguide. In particular, both numerical simulations [3, 4] and field experiments [5, 6] show that early portions of arrival patterns formed by steep rays manifest surprising stability. Due to this property, the ray travel time is the main signal parameter in the underwater acoustics experiments from which inversions is performed to reconstruct ocean temperature field [7, 8].

Our main objective is to develop an approximate analytical approach for description of the ray motion, including analysis of ray travel times, at very long ranges. We argue that this goal can be accomplished in the scope of a perturbation theory based on the Hamiltonian formalism in terms of the action-angle variables [9, 10]. Range variations of the refractive index in our propagation model are not adiabatic and we cannot use the adiabatic invariance of the action variable. Nevertheless, it turns out that, even at long ranges, the variance of the action variable is small enough to be considered as a small parameter in the problem.

In the present paper we derive an approximate analytic relation for the difference in travel times of two

rays one of which propagates in the perturbed waveguide and another one in the unperturbed waveguide. We also obtain approximate solutions to the stochastic Hamilton (ray) equations for the action and angle variables. These solutions are then applied to analyze statistics of ray travel times at ranges up to 3000 km.

Our attention is focused on the so-called timefront representing ray arrivals in the time-depth plane. We estimate the width of different branches (segments) of the timefront in the presence of perturbation and establish the criterion of nonoverlapping of neighboring segments. It is also shown that the perturbation causes not only a widening (dispersion) of timefront segments but some regular bias of the segments as well. The estimation of this bias is also presented. Predictions made with our approximate analytical approach are verified by comparison to results of numerical simulations.

Note, that in the present paper we consider only internal-wave-induced perturbations. An important issue of travel time biases due to mesoscale inhomogeneities (see, e.g., Ref. [11]) has not been broached here.

The paper is organized as follows. The ray (Hamilton) equations in terms of the position-momentum variables,  $(p, z)$ , as well as environmental model on which we rely in this paper are presented in Sec. 2. The emphasis in this section is on discussion of properties of timefronts obtained by numerical solution of the ray equations. The action-angle canonical variables,  $(I, \theta)$ , are introduced in Sec. 3. Section 4 presents the derivation of our main relation for the difference in travel times,  $\Delta t$ , of perturbed and unperturbed rays. In Sec. 5 we deduce approximate stochastic equations governing fluctuations of action and angle variables due to random inhomogeneities. Solving this equation yields statistical characteristics of  $I$  and  $\theta$ . In Sec. 6 these characteristics are used to analyze relative magnitudes of different constituents of  $\Delta t$  and significantly simplify the expression for  $\Delta t$  by neglecting small terms. Our final expression for travel time variations is applied to investigation of the timefront structure. This is done in Sec. 7. Section 8 is concerned with generalization of the analytical approach to a more realistic environmental model. Our results are summarized in the final section. In

the Appendix we shortly discuss how the transformation from  $(p, z)$  to  $(I, \theta)$  variables can be performed numerically using a standard ray code.

## 2 Timefronts in the presence of internal-wave-induced perturbation

### 2.1 Ray dynamics in terms of the Hamiltonian formalism

Consider wave propagation in a two-dimensional medium with the coordinates  $r$  (range) and  $z$  (depth). It is assumed that the  $z$ -axis is directed downward and the plane  $z = 0$  is the sea surface. The ray trajectory  $z(r)$  is determined by the sound speed field  $c(r, z)$  and can be found from Fermat's principle [12, 10, 13, 14] according to which the first variation of the functional

$$S = c_r \int \frac{ds}{c(r, z)} = \int dr n(r, z(r)) \sqrt{1 + \left(\frac{dz}{dr}\right)^2}, \quad (1)$$

vanishes at the ray trajectory. Here  $n(r, z) = c_r/c(r, z)$  is the refractive index,  $c_r$  is a reference sound speed, and  $ds = dr \left(1 + (dz/dr)^2\right)^{1/2}$  is the arc length. The functional  $S$  represents the so-called eikonal and is related to the ray travel time,  $t$ , by

$$t = S/c_r. \quad (2)$$

Formally considering Eq. (1) as an action function of some mechanical system with the  $r$ -variable playing the role of time, one can apply the standard relations of classical mechanics [10, 12, 13]. This yields explicit expressions for the momentum,

$$p = n \frac{dz/dr}{\sqrt{1 + (dz/dr)^2}}, \quad (3)$$

and the Hamiltonian,

$$H = -\sqrt{n^2 - p^2}. \quad (4)$$

Equations  $p = n \sin \chi$  and  $H = -n \cos \chi$  relate the momentum and the Hamiltonian to the ray grazing angle,  $\chi$  [4].

Expression (1) for the eikonal can now be rewritten as

$$S = \int (pdz - Hdr). \quad (5)$$

Ray trajectories are governed by the Hamilton equations [3, 4]

$$\frac{dz}{dr} = \frac{\partial H}{\partial p} = -\frac{p}{H} = \frac{p}{\sqrt{n^2 - p^2}}, \quad (6)$$

$$\frac{dp}{dr} = -\frac{\partial H}{\partial z} = \frac{n \partial n / \partial z}{\sqrt{n^2 - p^2}}. \quad (7)$$

Equation (1)-(7) present the Hamiltonian formalism in terms of the momentum-position canonical variables. Later on (in Sec. 3) we shall introduce another pair of canonical variables, namely, the action-angle variables.

## 2.2 Environmental model

In what follows we shall consider a model of the sound speed field in the form

$$c(r, z) = c_0(z) + \delta c(r, z), \quad (8)$$

where  $c_0(z)$  is a smooth (background) sound speed profile, and  $\delta c(r, z)$  is a range-dependent perturbation.

The unperturbed profile  $c_0(z)$  used in our numerical simulation is typical for deep water acoustic waveguides. It is shown in the left panel of Fig. 1. The sound-channel axis, i.e. minimum of the sound speed profile, is located at a depth of 0.738 km.

We consider an internal-wave-induced sound speed perturbation,  $\delta c(r, z)$ , with a zero mean ( $\langle$

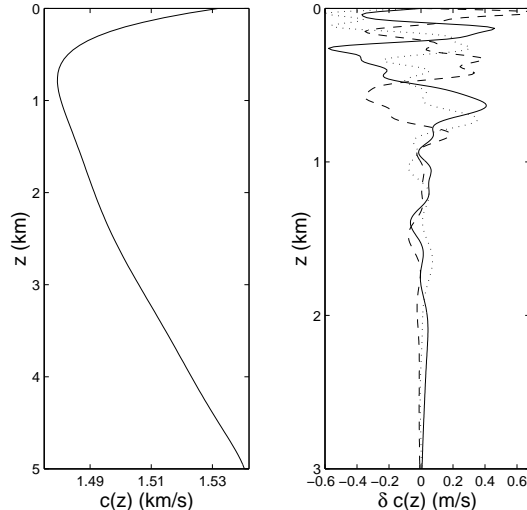


Figure 1: Left panel: Background sound speed profile. Right panel: Sound speed perturbation versus depth at three different ranges.

$\delta c(r, z) \geq 0$ ) and assume that the statistics of the internal wave field is described by the empirical Garrett-Munk spectrum [1]. A numerical technique for generation of such perturbations developed by J. Colosi and M. Brown [2] has been applied. Equations (1) and (19) from Ref. [2] have been used to generate a particular realization of  $\delta c(r, z)$  which is used throughout this paper. It has been assumed that the buoyancy frequency profile  $\nu(z)$  is exponential,  $\nu(z) = \nu_0 \exp(-z/B)$ , and determined by two constants: a surface-extrapolated buoyancy frequency  $\nu_0 = 2\pi/10 \text{ min}^{-1}$  and a thermocline depth scale  $B = 1 \text{ km}$ . We consider the internal wave field formed by 30 normal modes and assume its horizontal isotropy. Components of wave number vectors in the horizontal plane belong to the interval from  $2\pi/100 \text{ km}^{-1}$  to  $2\pi/4 \text{ km}^{-1}$ . An rms amplitude of the perturbation,  $(\delta c)_{\text{rms}}$ , scales in depth like  $\exp(-3z/2B)$  and its surface-extrapolated value in our model is about 0.5 m/s. Depth dependencies of  $\delta c$  at three different ranges are shown in the right panel of Fig. 1.

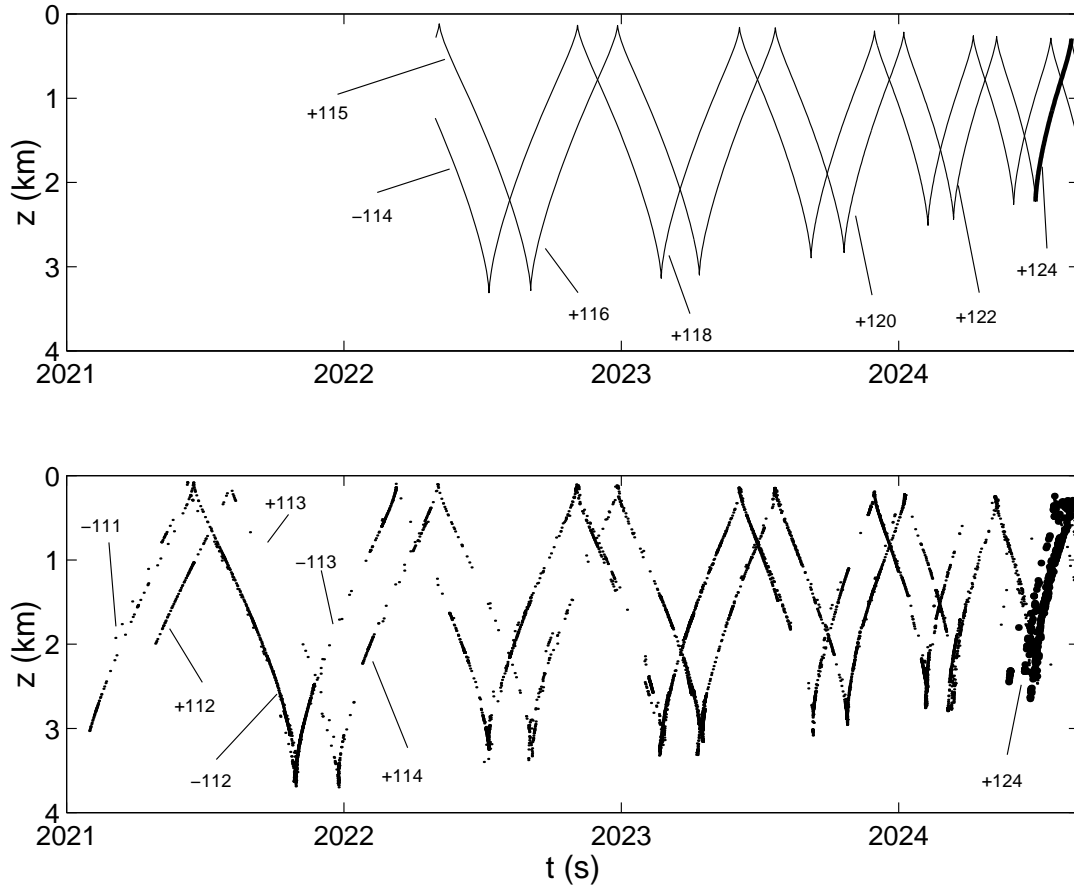


Figure 2: Early portion of the timefront at the range 3000 km without (upper panel) and with (lower panel) internal waves present. Identifiers of rays forming some particular segments are indicated next to the corresponding segments. In the upper panel, arrivals with identifier +124 are depicted by a thick solid line. In the lower panel, arrivals with this identifier are marked by thick points.

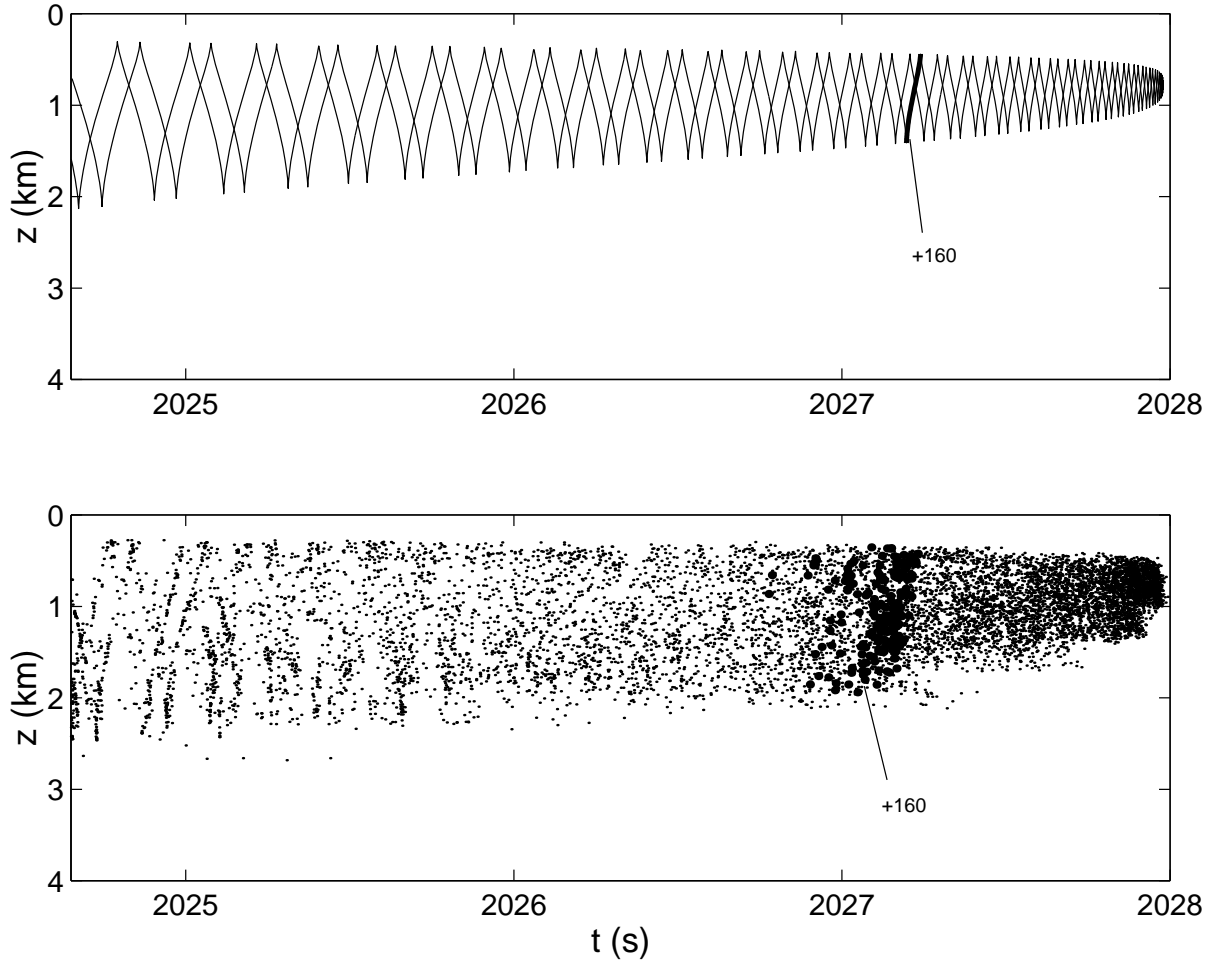


Figure 3: Late portion of the timefront at the range 3000 km without (upper panel) and with (lower panel) internal waves present. In the upper panel, arrivals with identifier +160 are depicted by a thick solid line. In the lower panel, arrivals with this identifier are marked by thick points.

### 2.3 Numerical simulation of timefronts

Figures 2 and 3 show early and late portions of the timefront at 3000 km ranges, respectively, for rays escaping a point source set at a depth of 0.78 km. The timefront in the unperturbed waveguide graphed in the upper panels of Figs. 2 and 3 has been computed using a fan of 16000 rays with starting momenta equally spaced within an interval corresponding to launch angles  $\pm 12^\circ$ . The timefronts in the perturbed waveguide has been produced by tracing 49000 rays with starting momenta covering the **same** interval.

The timefront in the range-independent waveguide has the well-known accordion-like shape consisting of smooth segments (branches) [4, 15]. Each segment is formed by points corresponding to arrivals of rays with the same identifier  $\pm J$ , where  $J$  is the number of ray turning points and symbols  $+$  and  $-$  correspond to rays starting upward and downward, respectively. So, we can associate each segment with the identifier of rays forming this segment. Identifiers for some particular segments in the unperturbed waveguide are indicated in the upper panels of Figs. 2 and 3. It is seen that the travel time grows with  $J$ . This is a typical situation for a deep water waveguide [15]: steep rays usually have greater cycle lengths (smaller  $J$ ) and arrive earlier than flat ones. Segments corresponding to rays with launch angles of the same sign form a broken line. Two such lines shifted along the  $t$ -axis form the unperturbed timefront (see plots in the upper panels of Figs. 2 and 3).

A very interesting and important feature of the perturbed timefronts is a remarkable stability of segments formed by early arriving steep rays. This property of steep rays is well-known and it has been observed in both numerical simulations and field experiments [3, 4, 5, 6].

Figure 4 presents the ray travel time,  $t$ , as a function of  $\chi_s$ , magnitude of the launch angle. Here and in the remainder of the paper we present numerical results only for rays starting upward (for rays starting downward the results are absolutely the same). In the range-independent case the function  $t(\chi_s)$  is smooth and monotonous (solid curve). In contrast,

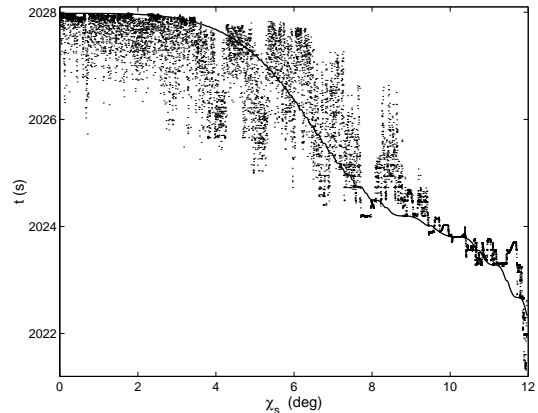


Figure 4: Ray travel times at the range of 3000 km as a function of launch angle, without (solid line) and with (points) internal waves present.

for the range-dependent case, we observe strong sensitivity of ray travel time to starting angles: points depicting travel times of perturbed rays are randomly scattered. Another manifestation of stochastic ray instability in the presence of internal waves is seen in Fig. 5 where the ray identifier at 3000 km range is shown as a function of the launch angle. Perturbed rays with close initial conditions may have quite different number of cycles. Although steep rays look less chaotic compared to flat ones (see Fig. 4 and the upper panel in Fig. 5), a magnified view of the angular interval  $\chi_s > 9^\circ$  shown in the lower panel of Fig. 5 demonstrates that the dependence of  $J$  on  $\chi_s$  for steep rays in the perturbed waveguide is also split into a set of irregular stripes.

The time spread,  $\delta t$ , for rays with close launch angles in the perturbed waveguide can be estimated as a width of the area occupied by randomly scattered points in Fig. 4. For rays with  $\chi_s < 9^\circ$  this yields  $\delta t \approx 1.5$  s. However, if we select a group of arrivals corresponding to rays with the given identifier, we shall find that the time spread of these arrivals will be significantly less than  $\delta t$ . It is seen in Figs. 2 and 3 where two such groups of arrivals are shown by thick points.

So, in spite of strong sensitivity of ray parameters

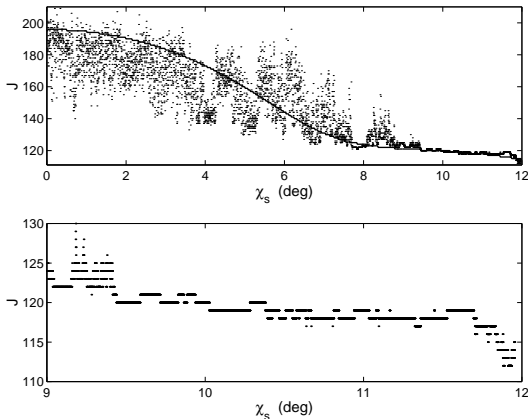


Figure 5: Points in the top figure show the ray identifier at the range 3000 km as a function of launch angle, in the presence of internal waves. The bottom figure presents a magnified view of this dependence for steep rays taken directly from the top figure. The solid line in the top figure graphs the dependence  $J(\chi_s)$  in the unperturbed waveguide.

to initial conditions, numerical simulations demonstrate an unexpectedly small time spread for rays with the given identifier. Loosely, we can state that although the ray travel time exhibits a chaotic and unpredictable dependence on the launch angle, its dependence on the ray identifier is much more predictable. This effect is most apparent for steep rays which form segments of the perturbed timefront almost coinciding with the corresponding segments of the unperturbed timefront. However, this fact does not mean that steep rays with the same launch angle in the perturbed and unperturbed waveguides follows close ray paths.

To illustrate this statement and demonstrate that the situation is much more reach and interesting come back to Fig. 2. Note that the perturbed timefront begins earlier than the unperturbed one and six earliest segments in the lower panel of Fig. 2 with identifiers  $-111$ ,  $\pm 112$ ,  $\pm 113$ , and  $+114$  have no counterparts in the upper panel. The point is that rays with these identifiers in the unperturbed waveguide have launch angles exceeding the maximum launch angle in our

fan. In the presence of perturbation such rays appear (see horizontal stripes with  $J = 112$ ,  $113$ , and  $114$  in both panels of Fig. 5 at  $\chi_s$  close to  $12^\circ$ ) because perturbation leads to widening of the interval of ray grazing angles. As it has been indicated already, in our waveguide steep rays arrive earlier than flat ones. So, it is natural that in the presence of perturbation we observe rays arriving earlier than those from the unperturbed fan. However, it is surprising and absolutely unexpected that steep rays which appeared due to scattering at random inhomogeneities, form quite regular segments. Moreover, these segments coincide with the unperturbed segments missed in the upper panel of Fig. 2.

One of our objectives is to explain how chaotic behavior of ray paths is compatible with stability of early portions of the timefront formed by steep rays and with unexpectedly small time spread of clusters of flat rays. Later on, we shall address these issues using the Hamiltonian formalism in terms of the action-angle canonical variables [9, 10]. The action-angle variables are introduced in the next section.

### 3 Action-angle variables

#### 3.1 Range-independent waveguide

First, we define the action-angle variables in a range-independent waveguide with  $c = c_0(z)$  and, correspondingly,  $n = c_r/c_0(z) = n_0(z)$ . In such a waveguide the Hamiltonian remains constant along the ray trajectory:

$$H_0 = -\sqrt{n_0^2(z) - p^2}. \quad (9)$$

This is the Snell's law [15, 14] (in geometrical optics it is often presented in the form  $n_0(z) \cos \chi = \text{const}$ ) analogous to the energy conservation law in classical mechanics. Equation (9) establishes a simple relation between the momentum  $p$  and coordinate  $z$

$$p = \pm \sqrt{n_0^2(z) - H_0^2}. \quad (10)$$

The action variable  $I$  is defined as the integral [9,

10]

$$I = \frac{1}{2\pi} \oint p dz = \frac{1}{\pi} \int_{z_{\min}}^{z_{\max}} dz \sqrt{n_0^2(z) - H_0^2} \quad (11)$$

running over the cycle of ray trajectory. Here  $z_{\min}$  and  $z_{\max}$  are the depths of upper and lower ray turning points, respectively. Equation (11) determines “energy”,  $H_0$ , as a function of the action variable,  $I$ . Note the relation

$$\frac{dH_0}{dI} = \frac{2\pi}{D} = \omega, \quad (12)$$

where

$$D = -2H_0 \int_{z_{\min}}^{z_{\max}} \frac{dz}{\sqrt{n_0^2(z) - H_0^2}} \quad (13)$$

is the cycle length of the ray path, and  $\omega$  is the angular frequency of spatial path oscillations. Equation (13) follows from (6), (10), and (11).

The canonical transformation from the position-momentum,  $(p, z)$ , to the action-angle,  $(I, \theta)$ , variables

$$I = I(p, z), \quad \theta = \theta(p, z) \quad (14)$$

and the inverse transformation

$$z = z(I, \theta), \quad p = p(I, \theta) \quad (15)$$

are determined by the equation [9]

$$dS = pdz - H_0 dr = dG - \theta dI - H_0 dr, \quad (16)$$

where  $G = G(I, z)$  is the generating function. An explicit expression for  $G(I, z)$  is well-known [9, 10]. We represent it in the form

$$G(I, z) = \begin{cases} \int_{z_{\min}}^z dz \sqrt{n_0^2(z) - H_0^2(I)}, & p > 0 \\ 2\pi I - \int_{z_{\min}}^z dz \sqrt{n_0^2(z) - H_0^2(I)}, & p < 0 \end{cases}, \quad (17)$$

where  $z_{\min}$  and  $z_{\max}$  are considered as functions of  $I$ . Then, equations

$$p = \frac{\partial G}{\partial z} = \pm \sqrt{n_0^2(z) - H_0^2(I)}, \quad (18)$$

and

$$\theta = \frac{\partial G}{\partial I}$$

$$= \begin{cases} \frac{2\pi H_0(I)}{D} \int_{z_{\min}}^z \frac{dz}{\sqrt{n_0^2(z) - H_0^2(I)}}, & p > 0 \\ 2\pi - \frac{2\pi H_0(I)}{D} \int_{z_{\min}}^z \frac{dz}{\sqrt{n_0^2(z) - H_0^2(I)}}, & p < 0 \end{cases} \quad (19)$$

define the transformations Eqs. (14) and (15).

Note, that the so defined angle variable  $\theta$  varies from 0 to  $2\pi$  at each cycle of the trajectory. We assume that the cycle begins at the minimum of the trajectory. To make the angle variable continuous, its value should be increased by  $2\pi$  at the beginning of each new cycle. It should be emphasized that both functions in Eq. (15) are periodic in  $\theta$  with period  $2\pi$ .

The ray equations in the new variables take the trivial form

$$\frac{dI}{dr} = -\frac{\partial H_0}{\partial \theta} = 0, \quad \frac{d\theta}{dr} = \frac{\partial H_0}{\partial I} = \omega(I) \quad (20)$$

with the solution

$$I = I_s, \quad \theta = \theta_s + \omega(I_s) r, \quad (21)$$

where  $I_s$  and  $\theta_s$  are starting values of the action and angle variables, respectively, at  $r = 0$ .

Let us emphasize an almost trivial point which, nonetheless, is crucial for our subsequent analysis. Although canonical transformations (14) and (15) are determined by the function  $n_0(z)$ , formally, they can be applied in a waveguide with a **different** refractive index profile. Moreover, these transformations can be used in a range-dependent waveguide, as well.

### 3.2 Range-dependent waveguide

Turn our attention to a more realistic model of the sound speed field given by Eq. (8). In this range-dependent environment with  $n(r, z) = c_r/c(r, z)$  we define the action-angle variables using the same relations as in the unperturbed waveguide with the refractive index  $n_0(z) = c_r/c_0(z)$ .

Rewrite the Hamiltonian  $H = -\sqrt{n^2 - p^2}$  in the form

$$H = H_0 + V, \quad (22)$$

with  $H_0(p, z)$  defined by Eq. (9) and

$$V(p, z, r) = -\sqrt{n^2(z, r) - p^2} + \sqrt{n_0^2(z) - p^2}. \quad (23)$$

Since our generating function  $G$  does not depend explicitly on  $r$ , the Hamiltonian in the new variables  $(I, \theta)$  is obtained by simple substitution of functions (15) into the above equations. This yields

$$H(I, \theta, r) = H_0(I) + V(I, \theta, r). \quad (24)$$

An explicit expression for the action function (eikonal) is obtained by integrating Eq. (16) with  $H_0$  replaced by  $H$ . We rewrite this equation as

$$dS = d(G - \theta I) - Id\theta - Hdr \quad (25)$$

and note that even though  $G$  and  $\theta$  are discontinuous at minima of the ray trajectory, the term  $G - \theta I$  vanishes at these points and, so, this term varies continuously along the ray. The eikonal for a ray connecting points  $(0, z_s)$  and  $(r, z_e)$  can be represented in the form

$$S = \int (Id\theta - Hdr)$$

$$-G(z_s, I_s) + G(z_e, I_e) + \theta_s I_s - \theta_e I_e, \quad (26)$$

where  $\theta_s$  and  $\theta_e$  are angle variables at ranges 0 and  $r$ , respectively. They are defined by Eq. (19) with  $z$ ,  $I$ , and  $p$  being ray parameters at the beginning and at the end of the path. Note, that the subscript 's' marks starting ray parameters while 'e' marks parameters at the end of the trajectory. This notation will be used throughout the paper.

In what follows we shall consider  $\theta$  as a continuous variable defined in accordance with the remark made after Eq. (19). Then

$$\theta(0) = \theta_s, \quad \theta(r) = 2\pi N + \theta_e, \quad (27)$$

where  $N$  is the number of minima of the ray path,  $\theta_s$  and  $\theta_e$  are the same quantities as in Eq. (26) ( $0 \leq \theta_s, \theta_e \leq 2\pi$ ).

The Hamilton equations now take the form

$$\frac{dI}{dr} = -V_\theta, \quad (28)$$

and

$$\frac{d\theta}{dr} = \omega + V_I, \quad (29)$$

where

$$V_\theta \equiv \frac{\partial V}{\partial \theta}, \quad V_I \equiv \frac{\partial V}{\partial I}.$$

Two comments should be made to this definition of the action-angle variables.

(i) The action variable introduced in this way (we have followed Refs. [10, 13]) does not conserve along the ray path even in a waveguide with very smooth range-dependence, i.e. our actions are not adiabatic invariants. Another definition of these variables [9] where the action does have a property of adiabatic invariance is shortly described in Sec. 8.

(ii) Splitting of the Hamiltonian into a sum of the unperturbed constituent,  $H_0$ , and the perturbation,  $V$ , have been made in anticipation of our later use of a perturbation expansion based on smallness of  $\delta c$  and, hence,  $V$ . However, for now we have not assumed the perturbation to be small and all equations derived so far are exact.

## 4 Explicit expression for difference in ray travel times

In this section we compare two rays one of which propagates in an unperturbed range-independent waveguide with  $\delta c = 0$ , while another one propagates in a range-dependent waveguide with nonzero  $\delta c$ . Both rays start at  $r = 0$  and our task is to derive an analytical relation for the difference in their travel times at a given range  $r > 0$ . Starting parameters of the rays are, generally, different but we assume

that their action variables remain more or less close at any intermediate range. This assumption will be quantified later on.

To distinguish between similar parameters of the two rays under consideration, parameters of a ray in the unperturbed waveguide will be marked with the overbar. For example, starting and final parameters of its trajectory will be denoted by  $(\bar{p}_s, \bar{z}_s)$  and  $(\bar{p}_e, \bar{z}_e)$ , respectively, while for another ray we shall write  $(p_s, z_s)$  and  $(p_e, z_e)$ .

The symbol  $\Delta$  will be used to denote the difference between any characteristic of one ray and its counterpart for another ray, e.g.  $\Delta I = I - \bar{I}$ ,  $\Delta S = S - \bar{S}$ ,  $\Delta z_s = z_s - \bar{z}_s$ , and so on.

#### 4.1 Difference in eikonals

Presenting Eq. (29) in the form

$$d\theta = (\omega + V_I) dr \quad (30)$$

and substituting it into Eq. (26) we transform the expression for the eikonal to

$$S = S_G + S_0 + S_V, \quad (31)$$

where

$$S_G = -G(z_s, I_s, 0) + I_s \theta_s + G(z_e, I_e, r) - I_e \theta_e, \quad (32)$$

$$S_0 = \int (I\omega - H_0) dr, \quad (33)$$

$$S_V = \int (IV_I - V) dr. \quad (34)$$

Equations (27) and (30) yield

$$2\pi N + \theta_e - \theta_s = \int (\omega + V_I) dr. \quad (35)$$

For a ray in the unperturbed waveguide ( $V = 0$ ) the action  $\bar{I}$  does not depend on range and Eqs. (31)–(35) translate to

$$\bar{S} = \bar{S}_G + \bar{S}_0, \quad (36)$$

$$\bar{S}_G = -G(\bar{z}_s, \bar{I}, 0) + G(\bar{z}_e, \bar{I}, r) + (\bar{\theta}_s - \bar{\theta}_e)\bar{I}, \quad (37)$$

$$\bar{S}_0 = \int (\bar{I}\bar{\omega} - \bar{H}_0) dr, \quad (38)$$

$$2\pi\bar{N} + \bar{\theta}_e - \bar{\theta}_s = \int \bar{\omega} dr. \quad (39)$$

Turn our attention to the difference in eikonals

$$\Delta S = S - \bar{S}$$

$$= S_G - \bar{S}_G + S_0 - \bar{S}_0 + S_V. \quad (40)$$

Replacing  $\theta_s - \theta_e$  and  $\bar{\theta}_s - \bar{\theta}_e$  by expressions following from Eqs. (35) and (39), and making use of Eqs. (33), (34), and (38) we arrive at

$$\begin{aligned} \Delta S = S_G - \bar{S}_G + 2\pi(N - \bar{N})\bar{I} \\ + \int F(\bar{I}, \Delta I, r) dr + \int (V_I \Delta I - V) dr, \end{aligned} \quad (41)$$

where

$$\begin{aligned} F(\bar{I}, \Delta I, r) = \omega(\bar{I} + \Delta I, r)\Delta I \\ - H_0(\bar{I} + \Delta I, r) + H_0(\bar{I}, r). \end{aligned} \quad (42)$$

Note that the Taylor expansion of  $F$  in  $\Delta I$ ,

$$\begin{aligned} F(\bar{I}, \Delta I, r) = \frac{1}{2}\bar{\omega}'\Delta I^2 + \\ \frac{1}{3}\bar{\omega}''\Delta I^3 + \frac{1}{8}\bar{\omega}'''\Delta I^4 + \dots, \end{aligned} \quad (43)$$

where

$$\omega' = \frac{d\omega}{dI}, \quad \omega'' = \frac{d^2\omega}{dI^2}, \quad \omega''' = \frac{d^3\omega}{dI^3}, \quad (44)$$

begins with the second order term.

## 4.2 Constituents of travel time variation

The difference in travel times of our two rays,  $\Delta t = \Delta S/c_r$ , can be represented as a sum of 6 constituents:

$$\Delta t = \Delta t_N + \Delta t_I + \Delta t_V + \Delta t_{IV} + \Delta t_G + \Delta t_{se}, \quad (45)$$

where

$$c_r \Delta t_N = 2\pi(N - \bar{N})\bar{I}, \quad (46)$$

$$c_r \Delta t_I = \int \left( \frac{1}{2} \bar{\omega}' \Delta I^2 + \frac{1}{3} \bar{\omega}'' \Delta I^3 + \frac{1}{8} \bar{\omega}''' \Delta I^4 + \dots \right) dr, \quad (47)$$

$$c_r \Delta t_V = - \int V dr, \quad (48)$$

$$c_r \Delta t_{IV} = \int V_I \Delta I dr, \quad (49)$$

$$c_r \Delta t_G = -G(z_s, I_s) + G(\bar{z}_s, \bar{I}_s)$$

$$+G(z_e, I_e) - G(\bar{z}_e, \bar{I}) + \theta_s \Delta I_s - \theta_e \Delta I_e \quad (50)$$

The *exact* expression for  $\Delta t$  given by Eqs. (45) – (50) is very complicated. Fortunately, the constituents of  $\Delta t$  usually have quite different magnitudes. In the next section we obtain approximate solutions to stochastic ray equations in terms of action and angle variables. These solutions provide simple estimations of magnitudes of individual terms present in Eqs. (47)–(49). Then the expression for  $\Delta t$  can be significantly simplified by neglecting small terms. This is done in Sec. 6.

## 5 Stochastic ray dynamics in terms of action-angle variables

### 5.1 Stochastic equations for action and angle variables

Consider a particular ray with starting values of the action and angle variables equal to  $I_s$  and  $\theta_s$ , respectively. In the unperturbed waveguide, a trajectory with these initial conditions,  $\Gamma_0$ , is defined by Eqs. (21). In the presence of perturbation we write the action and angle variables as

$$I(r) = I_s + x(r), \quad (51)$$

and

$$\theta(r) = \theta_s + \omega(I_s)r + y(r) \quad (52)$$

where  $x$  and  $y$  describe a deviation of a real trajectory from  $\Gamma_0$ . Although the deviation can be significant – perturbed and unperturbed trajectories at the same range may have different number of cycles – we assume that the variation of the action variable,  $x$ , (but not  $y$ !) is small. Substituting the above equations into Eqs. (28) and (29) we replace  $\omega(I)$  by  $\omega(I_s) + \omega'(I_s)x$  and neglect  $x$  in  $V_\theta$  and  $V_I$ . Then we arrive at

$$\frac{dx}{dr} = -V_\theta(I_s, \theta_s + \omega(I_s)r + y, r), \quad (53)$$

and

$$\frac{dy}{dr} = \omega'(I_s)x$$

$$+V_I(I_s, \theta_s + \omega(I_s)r + y, r) \quad (54)$$

with initial conditions  $x(0) = 0$  and  $y(0) = 0$ . At long ranges  $y$  may be greater than  $2\pi$ . Nevertheless, we can omit it in the right hand sides of Eqs. (53) and (54). The point is that both  $V_\theta(I, \theta, r)$  and  $V_I(I, \theta, r)$  are periodic in  $\theta$  with the period  $2\pi$  and the variation of  $y$  at one cycle of the trajectory is small. On the other hand, the cycle length  $D$  (typically, a few tens

km) exceeds the horizontal correlation scale of  $\delta c$ . So, by neglecting  $y$  in arguments of  $V_I$  and  $V_\theta$  we do not change statistical properties of these functions. In this approximation Eqs. (53) and (54) reduce to

$$\frac{dx}{dr} = \xi(r), \quad (55)$$

$$\frac{dy}{dr} = \omega'(I_s) x + \eta(r), \quad (56)$$

where

$$\xi(r) = -V_\theta(I_s, \theta_s + \omega(I_s)r, r), \quad (57)$$

$$\eta(r) = V_I(I_s, \theta_s + \omega(I_s)r, r). \quad (58)$$

Note, that  $\xi(r)$  can be easily expressed through the coordinate and inclination of the unperturbed ray trajectory  $\Gamma_0$  in the small-angle approximation. Setting  $c_r = 1.5$  km/s we have both  $n$  and  $n_0$  close to unity and for  $|p| \ll 1$

$$V = -\delta n(r, z), \quad (59)$$

where

$$\delta n(r, z) = n(r, z) - n_0(z) = \frac{\delta c(r, z)}{c_r}. \quad (60)$$

Then

$$V_\theta|_{\Gamma_0} = -\delta n_z(r, z(I, \theta)) \frac{\partial z(I, \theta)}{\partial \theta} \Big|_{\Gamma_0}, \quad (61)$$

where

$$\delta n_z(r, z) \equiv \frac{\partial \delta n(r, z)}{\partial z}.$$

Representing the trajectory  $\Gamma_0$  in the form  $z = z_0(r)$ , and denoting its grazing angle by  $\chi_0$ , we replace  $\partial z(I, \theta)/\partial \theta|_{\Gamma_0}$  with

$$\frac{dz/dr}{d\theta/dr} \Big|_{\Gamma_0} = \frac{\tan \chi_0}{\omega(I)}$$

(it has been taken into account that  $I$  is constant along the trajectory  $\Gamma_0$ ) and substitute this in Eq. (61). This yields

$$\xi(r) = \frac{1}{\omega(I)} \delta n_z(r, z_0(r)) \tan \chi_0(r). \quad (62)$$

Stochastic equations (55) and (56) have solutions

$$x(r) = \int_0^r dr' \xi(r'), \quad (63)$$

and

$$y(r) = \omega'(I_s) \int_0^r dr' (r - r') \xi(r') + \int_0^r dr' \eta(r'). \quad (64)$$

At ranges  $r \gg D$ , both functions  $x(r)$  and  $y(r)$  are Gaussian (due to the central limit theorem) and their statistical properties are determined by correlation functions of  $\xi$  and  $\eta$ . Note that statistics of  $\xi$  and  $\eta$  does not depend on the starting angle variable  $\theta_s$  but does depend on the starting action  $I_s$  because this constant defines the shape of the trajectory  $\Gamma_0$ . For a given realization of  $\delta c(r, z)$  the correlation functions of  $\xi$  and  $\eta$  can be computed by numerically evaluating the integrals

$$K_\xi(I, \rho) = \frac{1}{R} \int_0^R \xi(r' + \rho) \xi(r') dr', \quad (65)$$

and

$$K_\eta(I, \rho) = \frac{1}{R} \int_0^R \eta(r' + \rho) \eta(r') dr', \quad (66)$$

for  $R \gg D$ . We have omitted the subscript 's' at  $I$  in the arguments of  $K_\xi$  and  $K_\eta$ . Integrals (65) and (66) should not depend significantly on a particular realization of  $\delta c$  and on a particular value of starting angle variable  $\theta_s$ . Our numerical results are consistent with this expectation. The correlation functions used in our subsequent estimations have been computed by evaluating integrals (65) and (66) over range  $R = 3000$  km for a particular realization of  $\delta c$  with averaging over 20 initial values of  $\theta_s$  equally spaced within the interval of 0 to  $2\pi$ .

## 5.2 Action variable as a Wiener process

A further simplification of equations for  $x$  and  $y$  will be done by idealizing  $\xi$  and  $\eta$  as white noises with

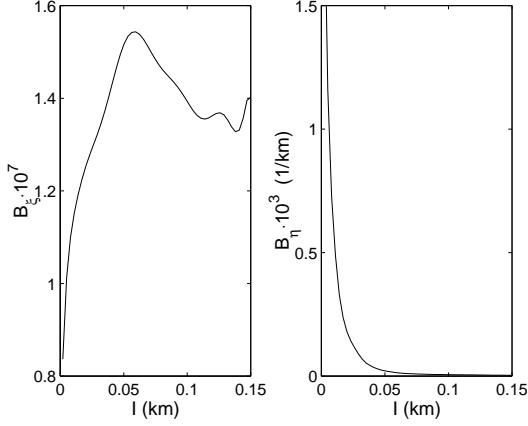


Figure 6: Coefficients  $B_\xi$  (left panel) and  $B_\eta$  (right panel) as functions of starting value of the action variable,  $I$ . The action  $I$  varies within the interval corresponding to launch angles of fan rays ( $0^\circ$  to  $+12^\circ$ ).

$$\langle \xi \rangle = 0, \quad \langle \xi(r)\xi(r') \rangle = B_\xi(I) \delta(r - r'), \quad (67)$$

and

$$\langle \eta \rangle = 0, \quad \langle \eta(r)\eta(r') \rangle = B_\eta(I) \delta(r - r'), \quad (68)$$

where

$$B_\xi(I) = \int_{-\infty}^{\infty} K_\xi(I, \rho) d\rho, \quad (69)$$

$$B_\eta(I) = \int_{-\infty}^{\infty} K_\eta(I, \rho) d\rho. \quad (70)$$

Figure 6 presents functions  $B_\xi(I)$  and  $B_\eta(I)$  computed for our environmental model in the interval of action variables corresponding to our ray fan. The computations have also demonstrated that the correlation of  $\xi(r)$  and  $\eta(r)$  is small and we assume

$$\langle \xi(r)\eta(r') \rangle = 0. \quad (71)$$

Equations (55) and (67) define  $x(r)$  as a Wiener process [16] with

$$\langle x \rangle = 0, \quad \langle x(r_1)x(r_2) \rangle = B_\xi(I) \min(r_1, r_2). \quad (72)$$

The variance of  $x$  is a linear function of range

$$\sigma_I^2 \equiv \langle x^2 \rangle = B_\xi r. \quad (73)$$

The same characteristic for  $y$  is

$$\sigma_\theta^2 \equiv \langle y^2 \rangle = (\omega')^2 B_\xi \frac{r^3}{3} + B_\eta r. \quad (74)$$

Here,  $\omega'$ ,  $B_\xi$ , and  $B_\eta$  are functions of the starting value of action,  $I$ , which is defined by starting depth and launch angle of the ray.

Figure 7 graphs standard deviations of action and angle variables, i.e.  $\sigma_I$  and  $\sigma_\theta$ , respectively, for a ray path starting at a depth of 0.78 km. Solid curves present results of averaging over a fan of 100 rays with launch angles from a narrow interval centered at  $\chi_c = 7.8^\circ$  (corresponding action  $I_c = 0.06$  km). Dashed curves show dependencies given by Eqs. (73) and (74). It is seen that the simple statistical model considered in this section provides reasonable predictions for standard deviations of  $x$  and  $y$ . Similar results have been obtained for rays starting at different launch angles.

Note, that for our environmental model the first term on the right in Eq. (74) is much greater than the second term. Thus, statistical characteristics of both action and angle variables are defined by a single coefficient  $B_\xi$ . It also means that the term  $\eta(r)$  in Eq. (56) is negligible and  $y(r)$  is approximately equal to an integral of the Wiener process  $x(r)$ , i.e.

$$y(r) = \omega'(I_s) \int_0^r x(r_1) dr_1. \quad (75)$$

Relations (72) – (75) describe statistics of a cluster of rays with launch angles close to some fixed value. This result will be used below in Sec. 7.

### 5.3 Cluster of rays with a given identifier

Now let us focus on a cluster of different type. Consider rays leaving a point source and arriving at the

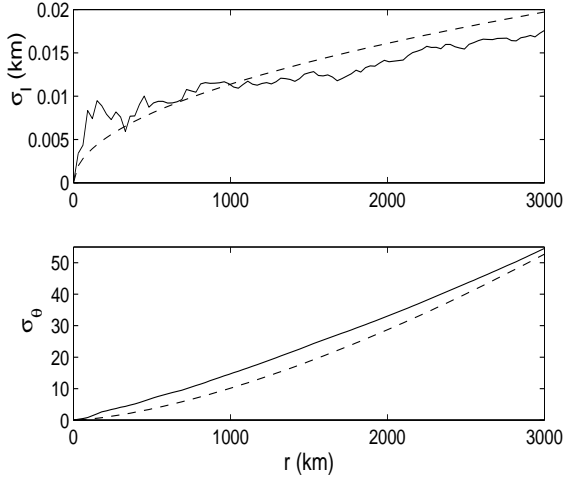


Figure 7: Standard deviations of the action (upper panel) and angle (lower panel) variables ( $\sigma_I$  and  $\sigma_\theta$ , respectively) as functions of range computed for a fan of 100 rays escaping a point source set at a depth of 0.78 km. Launch angles of the rays span a narrow angular interval centered at  $7.8^\circ$ . The solid curves present results of averaging over the fan rays. The estimation  $\sigma_I$  given by Eq. (73) is used to produce the dashed line in the upper panel. The dashed line in the lower panel is the estimation for  $\sigma_\theta$  given by Eq. (74).

given range  $r$  with the given identifier. Clusters of

this types with identifiers +124 and +160 form two groups of arrivals shown by thick points in Figs. 2 and 3, respectively.

To obtain an approximate analytical description of such clusters, compare two rays – one in the perturbed waveguide and another in the unperturbed waveguide – with close but, generally, different starting action variables. Using Eqs. (52) and (75), we present angle variables of these rays at the range  $r$  as

$$\theta = \theta_s + \omega(I_s)r + \omega'(I_s) \int_0^r x(r_1)dr_1$$

for the ray in the perturbed waveguide and

$$\bar{\theta} = \bar{\theta}_s + \omega(\bar{I})r$$

for the ray in the unperturbed waveguide. The difference  $\theta - \bar{\theta}$  can be approximated by the relation

$$\begin{aligned} \theta - \bar{\theta} &\simeq \int_0^r [\omega(I_s + x(r_1)) - \omega(\bar{I})] dr_1 \\ &\simeq \bar{\omega}'(I_s) \left( (I_s - \bar{I})r + \int_0^r x(r_1)dr_1 \right), \end{aligned} \quad (76)$$

where we have omitted the constant  $\theta_s - \bar{\theta}_s$ . At long ranges this constant becomes negligible compared to other terms whose rms magnitudes grow, on average, with  $r$ . Then the equation

$$\frac{1}{r} \int_0^r x(r_1)dr_1 = -I_s + \bar{I} \quad (77)$$

can be idealized as a condition that singles out rays whose identifiers at the range  $r$  are equal to the identifier of the unperturbed ray. Using this condition combined with Eqs. (51), (55) and (67), one can evaluate statistical characteristics of action variables of rays belonging to the cluster. To illustrate this statement we consider a couple of examples.

First, evaluate the probability density function (PDF)  $P(I_s)$ , defined in a following way:  $P(I_s)dI_s$  is a probability that a stochastic ray with a starting action within the interval of  $I_s$  to  $I_s + dI_s$  meets the

condition (77), i.e. this ray belongs to the cluster defined by Eq. (77). In other words, we consider  $I_s$  as a random variable and our task is to find its PDF.

It is well-known that the PDF of a random variable  $\beta$  can be presented in the form

$$P(b) = \langle \delta(b - \beta) \rangle \quad (78)$$

where the angular brackets denote the ensemble averaging operation. Note, that we denote any PDF by the same symbol  $P$  with an argument indicating a specific random variable.

Making use of Eq. (78) yields

$$P(I_s) = \langle \delta \left( I_s - \bar{I} + \frac{1}{r} \int_0^r x(r_1) dr_1 \right) \rangle, \quad (79)$$

where the averaging goes over trajectories of the Wiener process  $x(r)$  defined by Eqs. (55) and (67) with the initial condition  $x(0) = 0$ . Assuming that the width of  $P(I_s)$  is small compared to the scale of function  $B_\xi(I)$ , we replace  $B_\xi(I)$  in Eq. (67) by

$$\bar{B}_\xi \equiv B_\xi(\bar{I}). \quad (80)$$

In so doing we neglect the difference in statistical characteristics of rays with different starting values of actions.

Using the Fourier-representation of the  $\delta$ -function we rewrite Eq. (79) as

$$P(I_s) = \frac{1}{2\pi} \int_{-\infty}^{\infty} d\gamma e^{i\gamma(I_s - \bar{I})} \langle e^{i\frac{\gamma}{r} \int_0^r x(r_1) dr_1} \rangle. \quad (81)$$

The integral

$$g = \frac{1}{r} \int_0^r x(r_1) dr_1 \quad (82)$$

is a Gaussian random variable with zero mean,  $\langle g \rangle = 0$ . The average in the integrand on the right of Eq. (81) can be rewritten as [17]

$$\langle e^{i\gamma g} \rangle = e^{-\frac{\gamma^2}{2} \langle g^2 \rangle}. \quad (83)$$

Substituting Eq. (83) in Eq. (81) we arrive at a Gaussian integral over  $\gamma$ . Evaluating this integral

and applying Eq. (72) to find  $\langle g^2 \rangle$  yields

$$P(I_s) = \sqrt{\frac{3}{2\pi\bar{B}_\xi r}} \exp \left[ -\frac{3}{2} \frac{(I_s - \bar{I})^2}{\bar{B}_\xi r} \right]. \quad (84)$$

The standard deviation of  $I_s$  from its mean value  $\bar{I}$  is given by

$$\sigma_{I_s} = \sqrt{\bar{B}_\xi r/3}. \quad (85)$$

According to the plot in the left panel of Fig. 6 the value of  $\bar{B}_\xi$  can be approximately estimated as  $10^{-7}$  km. Then at 3000 km range we get  $\sigma_{I_s} \simeq 10^{-2}$  km which is consistent with our assumption made when replacing  $B_\xi(I)$  by  $\bar{B}_\xi$ . Let us emphasize an important point. This assumption implies that statistical characteristics of  $x$  for every rays from our cluster is defined by the value of action  $\bar{I}$  determining the cluster.

In the scope of our statistical model the difference in actions  $\Delta I(\rho) = I - \bar{I}$  present in equations for  $\Delta S$  and  $\Delta t$  derived in Sec. 4, is a Gaussian random function with a zero mean whose statistical characteristics are completely determined by the correlation function [17]

$$Q(\rho_1, \rho_2) = \langle \Delta I(\rho_1) \Delta I(\rho_2) \rangle. \quad (86)$$

Note, that  $\Delta I(\rho) = I_s + x(\rho) - \bar{I}$ . For short, we shall use the notation  $a_{1,2} = \Delta I(\rho_{1,2})$ . Applying again Eq. (78) we obtain the following expression for the joint PDF of  $I_s$ ,  $a_1$ , and  $a_2$  (it is assumed that  $0 \leq \rho_{1,2} \leq r$ ):

$$P(I_s, a_1, a_2) = \langle \delta(I_s - \bar{I} + g) \times \delta(a_1 - I_s + \bar{I} - x(\rho_1)) \delta(a_2 - I_s + \bar{I} - x(\rho_2)) \rangle. \quad (87)$$

Then

$$Q(\rho_1, \rho_2) = \int a_1 a_2 P(I_s, a_1, a_2) dI_s da_1 da_2$$

$$= \langle (x(\rho_1) - g)(x(\rho_2) - g) \rangle$$

$$= B \left( \frac{r}{3} - \rho_1 - \rho_2 + \frac{\rho_1^2 + \rho_2^2}{2r} + \min(\rho_1, \rho_2) \right). \quad (88)$$

Later on we shall use this equation to calculate statistical moments of  $\Delta I$  in order to estimate individual terms in the expansion (47). In so doing we shall apply the known properties of statistical momenta of Gaussian random variables [17]. In particular, we shall use the relation

$$\begin{aligned} \langle \Delta I^2(\rho_1) \Delta I^2(\rho_2) \rangle &= \langle \Delta I^2(\rho_1) \rangle \langle \Delta I^2(\rho_2) \rangle \\ &+ 2 \langle \Delta I(\rho_1) \Delta I(\rho_2) \rangle^2 \\ &= Q(\rho_1, \rho_1) Q(\rho_2, \rho_2) + 2Q^2(\rho_1, \rho_2). \quad (89) \end{aligned}$$

#### 5.4 Stochastic instability of ray identifier

In Sec. 2.3 we have already seen that in the perturbed waveguide ray trajectories exhibit extreme sensitivity to starting launch angles. An impressive demonstration of this instability is presented in Fig. 5. The points representing dependence of the ray identifier on the launch angle are randomly scattered and this fact suggests that rays with very close launch angles are practically uncorrelated and should be described statistically.

Our stochastic ray theory provides a tool for quantitative description of stochastic ray instability. In particular, it allows one to estimate chaotic spread of ray identifiers shown in Fig. 5. Consider unperturbed and perturbed rays starting at the same launch angle,  $\chi_s$ , and, consequently, with the same starting action,  $I_s$ . Denoting the numbers of turning points of these paths by  $\bar{J}$  and  $J$ , respectively, we note that at long ranges both  $\bar{J}$  and  $J$  are large and the same is true of their rms difference. Then we can approximate  $\Delta J = J - \bar{J}$  by  $y/2\pi$ . This yields  $\langle \Delta J \rangle = 0$  and  $\sigma_{\Delta J} \equiv (\langle \Delta J^2 \rangle)^{1/2} = \sigma_\theta/2\pi$  with  $\sigma_\theta$  given by Eq. (74). Assuming that for most rays with starting angles close to  $\chi_s$  the value of  $J$  lies within the interval

$$\bar{J} - 2\sigma_{\Delta J} < J < \bar{J} + 2\sigma_{\Delta J}, \quad (90)$$

we find an estimate for the spread of ray identifiers. Figure 8 presents the number of ray turning points,  $J$ , against the launch angle,  $\chi_s$ , at 1500 km and 3000 km. For 3000 km range we have the same plot as in Fig. 5, but the solid line representing the dependence of  $\bar{J}$  on  $\chi_s$  is slightly smoothed. The dashed lines represent limits defined by Eq. (90). This result confirms that Eq. (90) gives a rough estimation of the spread of ray identifiers.

Stochastic dependence of the identifier on the launch angle can be considered from a different viewpoint. Let us fix some ray identifier and study statistics of starting actions,  $I_s$ , of perturbed rays arriving at the given range  $r$  with this identifier. The probability density function of  $I_s$  is given by Eq. (84). The mean value of  $I_s$  is equal to  $\bar{I}$ , action of an unperturbed ray which has the given identifier at the range  $r$ . According to Eq. (84)  $I_s$  is a Gaussian random variable and it is natural to expect that most part of rays with the given identifier at range  $r$  have starting action within the interval

$$\bar{I} - 2\sigma_{I_s} < I_s < \bar{I} + 2\sigma_{I_s}, \quad (91)$$

where  $\sigma_{I_s}$  is determined by Eq. (85). Figure 9 demonstrates that this prediction agrees with results of our numerical simulation. The solid lines present dependencies of the starting action of the unperturbed ray on the number of ray turning points at 1500 km and 3000 km, while the dashed lines indicate the borders of intervals defined by Eq. (91). Consistent with our expectation, most points depicting parameters  $I_s$  of perturbed rays starting upward against numbers of their turning points at 1500 km (upper panel) and 3000 km (lower panel) lie within areas embraced by the dashed lines.

## 6 Small parameters in the problem and approximate formula for travel time variations

The approximate stochastic ray theory developed in the preceding section allows one to deduce simple analytical estimations of terms on the right side of Eq.

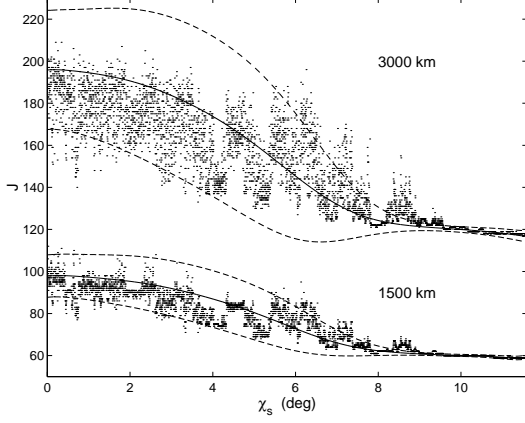


Figure 8: Ray identifier,  $J$ , as a function of the launch angle,  $\chi_s$ , at the ranges 1500 and 3000 km. The points depicting rays at 3000 km range are the same as in Figs. 2 and 3. The solid lines are smoothed functions  $J(\chi_s)$  for the unperturbed waveguide. The dashed lines show the limits established by Eq. (90)

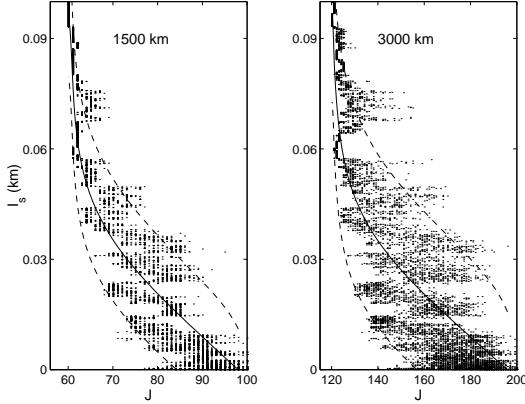


Figure 9: Starting action,  $I_s$ , as a function of ray identifier,  $J$ , for the ranges 1500 km (left) and 3000 km (right). The solid lines are smoothed functions  $I_s(J)$  for the unperturbed waveguide. The dashed lines show the limits established by Eq. (91).

(45). Our main concern is with terms  $\Delta t_I$ ,  $\Delta t_{IV}$ , and  $\Delta t_V$  which are given by integrals over  $r$  and, in principle, may be very large at long ranges. The objective of the present section is to compare these constituents of  $\Delta t$  and simplify Eq. (45) by neglecting small terms.

(i) **Estimation of  $\Delta t_I$ .** Divide  $\Delta t_I$  into a sum

$$\Delta t_I = \Delta t_I^{(2)} + \Delta t_I^{(3)} + \Delta t_I^{(4)} + \dots, \quad (92)$$

where

$$\Delta t_I^{(2)} = \frac{\bar{\omega}'}{2c_r} \int \Delta I^2 dr, \quad (93)$$

$$\Delta t_I^{(3)} = \frac{\bar{\omega}''}{3c_r} \int \Delta I^3 dr, \quad (94)$$

$$\Delta t_I^{(4)} = \frac{\bar{\omega}'''}{8c_r} \int \Delta I^4 dr, \quad (95)$$

and estimate mean values of components  $\Delta t_I^{(2)}$ ,  $\Delta t_I^{(3)}$ , and  $\Delta t_I^{(4)}$ . Applying Eq. (88) to find  $\langle \Delta I^2 \rangle$  and making use of the relation

$$\langle \Delta I^4 \rangle = 3 \langle \Delta I^2 \rangle^2 \quad (96)$$

valid for a Gaussian random variable with a zero mean (it follows from Eq. (89)), yields

$$\langle \Delta t_I^{(2)} \rangle = \frac{\bar{\omega}'}{12c_r} \bar{B}_\xi^2 r^2, \quad (97)$$

$$\langle \Delta t_I^{(3)} \rangle = 0, \quad \langle \Delta t_I^{(4)} \rangle = \frac{\bar{\omega}'''}{80c_r} \bar{B}_\xi^2 r^3. \quad (98)$$

(ii) **Estimation of  $\Delta t_{IV}$ .** Rewrite Eq. (49) as

$$\Delta t_{IV} = \frac{1}{c_r} \int \Delta I V_I dr = \frac{1}{c_r} \int x(r_1) \eta(r_1) dr.$$

Since  $\xi(r)$  and  $\eta(r)$  are uncorrelated (Eq. (71)), the term  $\Delta t_{IV}$  has a zero mean. We estimate  $\Delta t_{IV}$  by its standard deviation (square root of the variance)

from  $\langle \Delta t_{IV} \rangle = 0$ . Applying Eqs. (72) and (68), we obtain the variance of  $\Delta t_{IV}$

$$\begin{aligned} \langle (\Delta t_{IV})^2 \rangle &= \frac{1}{c_r^2} \int \int \langle x(r_1) x(r_2) \rangle \\ &\times \langle \eta(r_1) \eta(r_2) \rangle dr_1 dr_2 \\ &= \frac{r^2}{2c_r^2} \bar{B}_\xi \bar{B}_\eta, \end{aligned}$$

where the symbol  $\bar{B}_\eta$  by analogy with  $\bar{B}_\xi$  (see Eq. (80)) means  $B_\eta(\bar{I})$ .

**(iii) Estimation of  $\Delta t_V$ .** Consider the small-angle approximation and use Eq. (59), i.e. replace  $V$  in Eq. (48) with  $-\delta n(r, z)$ . Then

$$\Delta t_V = \frac{1}{c_r} \int_0^r \delta n(r, z(r)) dr. \quad (99)$$

Note a difference between  $\Delta t_V$  defined in Eq. (99) and a similar characteristic

$$\delta t_V = \frac{1}{c_r} \int_0^r \delta n(r, z_0(r)) dr, \quad (100)$$

where the integration goes over the unperturbed trajectory  $z_0(r)$ . The quantity  $\delta t_V$  is widely used to estimate travel time shifts due to inhomogeneities [1]. Since  $z_0(r)$  is independent of the random perturbation  $\delta n$  and  $\langle \delta n(r_1, z_1) \rangle = 0$  at any fixed point  $(r_1, z_1)$ , we find that  $\langle \delta t_V \rangle = 0$ . The variance of  $\delta t_V$  is given by

$$\langle \delta t_V^2 \rangle = \frac{r}{c_r^2} \int_{-\infty}^{\infty} d\rho K_{\delta n}(I, \rho), \quad (101)$$

where  $K_{\delta n}(I, \rho)$  is the correlation function which can be numerically evaluated using a realization of  $\delta n(r, z)$ :

$$\begin{aligned} K_{\delta n}(I, \rho) &= \frac{1}{R} \\ &\times \int_0^R \delta n(r, z_0(r)) \delta n(r + \rho, z_0(r + \rho)). \end{aligned} \quad (102)$$

In analogy to Eq. (71) the integration goes over a very long range  $R \gg D$ . The argument  $I$  defines the action variable of the unperturbed path  $z_0(r)$ . We shall use  $\langle \delta t_V^2 \rangle^{1/2}$  as an estimation of  $\Delta t_V$ . However, it should be emphasized that this estimation is rough. In particular, it can be shown that, generally,  $\langle \delta n(r, z(r)) \rangle \neq 0$  and, consequently,  $\langle \Delta t_V \rangle \neq 0$  (discussion of similar problems see, e.g., in Ref. [18]).

Applying the above estimations to our environmental model we have found that for most rays the sum  $\Delta t_I + \Delta t_V + \Delta t_{IV}$  up to, at least, 3000 km range can be approximately replaced with  $\Delta t_I^{(2)}$ . This approximation is valid if parameters

$$\mu_1 = \left| \frac{\langle \Delta t_I^{(4)} \rangle}{\langle \Delta t_I^{(2)} \rangle} \right| = \frac{3}{20} B_\xi r \left| \frac{\bar{\omega}'''}{\bar{\omega}'} \right|, \quad (103)$$

$$\mu_2 = \frac{\sqrt{\langle (\Delta t_{IV})^2 \rangle}}{\left| \langle \Delta t_I^{(2)} \rangle \right|} = \frac{6}{|\bar{\omega}'| r} \sqrt{\frac{2B_\eta}{B_\xi}}, \quad (104)$$

and

$$\mu_3 = \frac{\sqrt{\langle (\delta t_V)^2 \rangle}}{\left| \langle \Delta t_I^{(2)} \rangle \right|} = \frac{12\sqrt{B_{\delta n}}}{|\bar{\omega}'| B_\xi r^{3/2}} \quad (105)$$

are small compared to unity.

Note that only  $\mu_1$  grows with range. The other two parameters, in contrast, decrease with range. Taking into account Eq. (73) we can roughly estimate  $\mu_1$  as

$$\mu_1 \approx \frac{\sigma_I^2}{\delta I^2}, \quad (106)$$

where  $\delta I$  is a characteristic scale of function  $\omega(I)$ .

Figure 10 shows parameters  $\mu_1$ ,  $\mu_2$ , and  $\mu_3$  at the range 3000 km as functions of the launch angle for a point source set at a depth of 0.78 km. It is seen that while  $\mu_1$  and  $\mu_2$  are everywhere small, the parameter  $\mu_3$  is small only for flat enough rays.

This result suggests that the travel time difference  $\Delta t$  given by Eq. (45) can be approximated as

$$\Delta t = \Delta t_N + \Delta t_I^{(2)} + \Delta t_V + \Delta t_G. \quad (107)$$

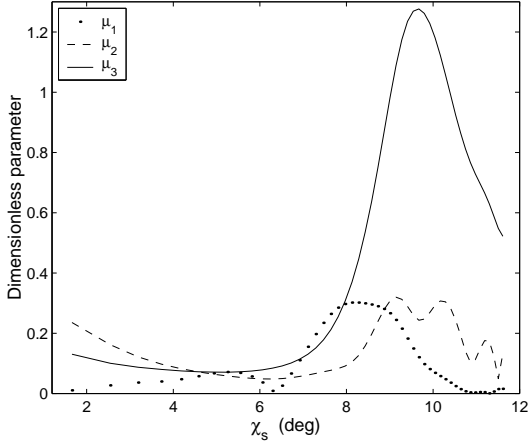


Figure 10: Dimensionless parameters defined by Eqs. (103)–(105) as functions of launch angle at the 3000 km range.

For flat enough rays the term  $\Delta t_V$  can be neglected and Eq. (107) further simplifies.

Consider the term  $\Delta t_G$  given by Eq. (50). First of all, recall that the function  $G$  depends not only on the ray coordinate  $z$  and action  $I$ , but on the sign of the momentum (grazing angle) at the given point as well (see Eq. (17)). In what follows we assume that perturbed and unperturbed rays under consideration have starting momenta of the same signs, and the same is true of their momenta at the end of trajectories. In other words we shall compare rays with identifiers  $+J$  and  $+J_1$  or  $-J$  and  $-J_1$  with even  $J - J_1$ . Then, in the case of a point source the sum of three terms in Eq. (50) depending on ray starting parameters is small. Indeed, in this case  $z_s = \bar{z}_s$  and applying Eq. (19) yields

$$-G(\bar{z}_s, I_s) + G(\bar{z}_s, \bar{I}) + \theta_s \Delta I_s = O(\Delta I_s^2).$$

If, in addition,  $\Delta z_e = 0$ , i.e.  $z_e = \bar{z}_e$  and we compare rays connecting the same points in the unperturbed and perturbed waveguides, the three remaining terms give  $O(\Delta I_e^2)$ . Assuming  $\Delta I_s$  and  $\Delta I_e$  to be small we can neglect  $\Delta t_G$ . If  $\Delta z_e$  is nonzero but small compared to the difference in ray turning depths,

$|z_{\max} - z_{\min}|$ , then applying Eqs. (18) and (19) yields

$$c_r \Delta t_G = \bar{p}_e \Delta z_e. \quad (108)$$

In what follows we shall apply Eq. (107) to study variations of the timefront due to internal-wave-induced random inhomogeneities. Our primary concern will be with the estimation of widening and bias of the timefront segments in the presence of perturbation.

## 7 Analytical description of timefront structure

### 7.1 Timefront in a range-independent waveguide

Although Eq. (107) has been derived to compare travel times of perturbed and unperturbed rays, it can also be applied in the case when both rays propagate in the unperturbed waveguide with  $\delta n = 0$ . Then the third term on the right in Eq. (107) vanishes, the action  $I$  (like  $\bar{I}$ ) does not depend on  $r$ , and the same is true of  $\Delta I$ . We shall compare rays arriving at the same points, i.e. eigenrays, and in accordance with Eq. (108) neglect the term  $\Delta t_G$ . This yields

$$c_r \Delta t = 2\pi \bar{I}(N - \bar{N}) + \frac{\bar{\omega}'}{2} \Delta I^2 r. \quad (109)$$

In the case  $N - \bar{N} = 1$  this equation provides a difference in travel times of two eigenrays with identifiers  $\pm J$  and  $\pm(J - 2)$ . According to Eqs. (21) and (27) the action variable of these eigenrays satisfies

$$\begin{aligned} \omega(I) - \omega(\bar{I}) &= \bar{\omega}' \Delta I + O(\Delta I^2) \\ &= \frac{1}{r} (2\pi - \Delta \theta_s + \Delta \theta_e). \end{aligned} \quad (110)$$

Assuming that  $\omega$  as a function of  $I$  is monotonous at the interval  $(I, \bar{I})$ , at long ranges ( $N \gg 1$ ) we have  $|\Delta \theta_s|, |\Delta \theta_e| \ll 2\pi$  and

$$\Delta I = \frac{2\pi}{\bar{\omega}' r} + O\left(\frac{1}{r^2}\right). \quad (111)$$

Then Eq. (109) reduces to

$$c_r \Delta t = \pi(I + \bar{I}). \quad (112)$$

A similar result have been obtained in Refs. [19, 20, 21] (in Refs. [19, 21] it has been derived for a adiabatically range-dependent waveguide).

An interesting and somewhat surprising fact following from (112) is that there exists a conservation law for temporal shifts between timefront segments. Consider a bunch of rays with launch angles within a narrow interval. Action variables of all these rays are close to some value which we denote by  $I_0$ . Beginning from a certain range  $r_*$  these rays will form at least two segments with identifiers that differ by 2. When estimating temporal shift between two such segments we shall compare rays arriving at the same depths. With this in mind, we can estimate the temporal shift as  $\tau_0 = 2\pi I_0/c_r$ . It should be emphasized that  $\tau_0$  does **not** depend on range. It means that although the number of segments formed by rays with launch angles from a given narrow angular interval grows linearly with range, temporal shifts between neighboring segments (to be more precise, between segments corresponding to identifiers  $\pm J$  and  $\pm(J-2)$  with  $J$  depending on range) remain approximately the same at any distance. A more detailed discussion of this issue is given in Refs. [19, 21].

The above statement means that a simple evaluation of the action variable as a function of launch angle,  $I(\chi)$ , gives a considerable quantitative information on temporal structure of the pulse signal valid at arbitrary (long enough) range. If  $N \gg 1$ , the values of  $I$  and  $\bar{I}$  on the right side of Eq. (112) are close and this equation can be approximated by

$$\Delta t = \tau \left( \frac{\chi_s + \bar{\chi}_s}{2} \right), \quad (113)$$

where  $\chi_s$  and  $\bar{\chi}_s$  are launch angles of rays under consideration and

$$\tau(\chi_s) = 2\pi I(\chi_s)/c_r. \quad (114)$$

A solid line in Fig. 11 graphs  $\tau(\chi_s)$  for our model of range-independent waveguide. Looking at this curve we can predict that, for example, a difference in travel

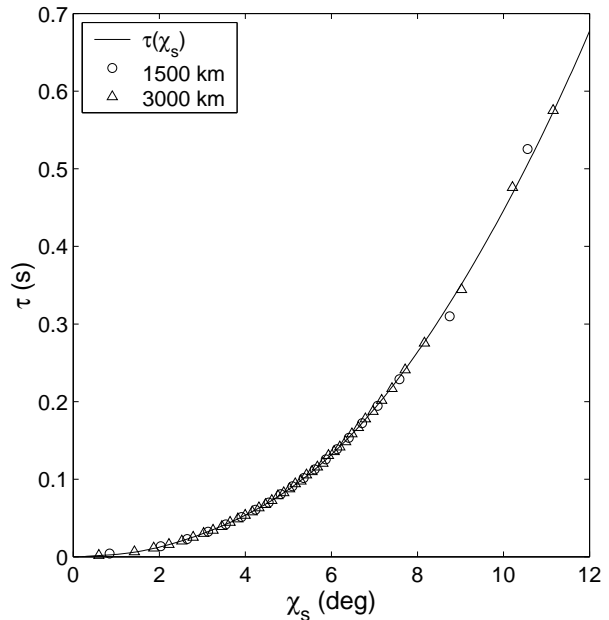


Figure 11: The solid curve is  $\tau = 2\pi I(\chi)/c_r$  from Eq. (114). The circles and triangles are time delays between segments with the identifiers  $+J$  and  $+(J-2)$  at a reference depth of 0.78 km computed for even  $J$  at 1500 km and 3000 km ranges, respectively.

times of two eigenrays with launch angles close to  $7^\circ$  and numbers of cycle which differ by 1, will be close to  $\tau = 0.19$  s at **any** range and at **any** depth, provided such eigenrays arrive at the observation point.

Let us select some reference depth,  $z_r$ , and define the temporal shift between segments with identifiers  $\pm J$  and  $\pm(J-2)$  – we denote this shift by  $T_{\pm J, \pm(J-2)}$  – as a difference in travel times of two eigenrays with these identifiers arriving at the depth  $z_r$ . Arrivals of these rays in the upper panels of Fig. 2 and 3 can be found as intersections of the corresponding segments with a horizontal line  $z = z_r$ . According to Eq. (114) the value of  $T_{\pm J, \pm(J-2)}$  does not depend on a particular value of  $z_r$  (the only requirement is that both segments must intersect the line  $z = z_r$ ). This result agrees with the fact that neighboring segments in Figs. 2 and 3 with inclinations of the same sign

are almost parallel.

Since  $T_{\pm J, \pm(J-2)}$  represent a difference in travel times of two eigenrays, it can be estimated as  $\tau(\chi_{\pm J, \pm(J-2)})$  with  $\chi_{\pm J, \pm(J-2)}$  being a half-sum of launch angles of the corresponding eigenrays. It means that points depicting values of  $T_{\pm J, \pm(J-2)}$  against  $\chi_{\pm J, \pm(J-2)}$  should lie on the curve  $\tau(\chi)$  at any range and for any reference depth,  $z_r$ . In Fig. 11 this prediction is verified for the timefront shown in the upper panels of Figs. 2 and 3 and for a similar timefront at the range of 1500 km. Circles and triangles depict  $T_{+J, +(J-2)}$  as functions of  $\chi_{+J, +(J-2)}$  at 1500 km and 3000 km ranges, respectively, for  $z_r = 0.78$  km. Travel times shifts for only even  $J$  (from 60 to 96 at 1500 km, and from 118 to 196 at 3000 km) are shown. It is clearly seen that all the circles and triangles are, indeed, located close to the solid curve representing  $\tau(\chi)$ .

## 7.2 Timefront in the presence of perturbation

### 7.2.1 Widening and bias of timefront segments

In the presence of weak range-dependent inhomogeneities the structure of timefront becomes more complicated: instead of infinitely thin segments of smooth curves, we have some areas filled with randomly scattered points. Although we observe the scattered points only because our fan is far too sparse to resolve what should be unbroken curves, the appearance of such regions indicates the presence of chaotic rays.

As it has been pointed out in Sec. 2.3 the early portion of the timefront formed by steep rays still “remembers” its structure in the unperturbed waveguide. The points depicting arrivals of rays with the given identifier are scattered in the vicinity of the corresponding unperturbed segment. A group of arrivals formed by rays with the same identifier produces a fuzzy version of an unperturbed segment. We shall call such groups of points in the time-depth plane, the fuzzy segments. Thus, every fuzzy segment, like every segment of the unperturbed timefront, is asso-

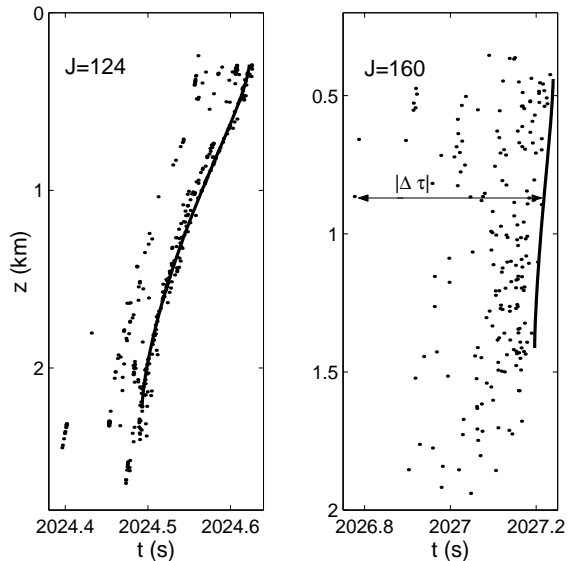


Figure 12: Arrivals with identifiers +124 (left panel) and +160 (right panel) at the range 3000 km presented in the time-depth plane. The points and solid lines depict arrivals with and without internal waves present, respectively. The magnitude of time delay,  $|\Delta\tau|$ , between arrivals of the perturbed ray and an unperturbed ray with the same identifier is shown for the earliest arrival with identifier +160.

ciated with some identifier. Two examples of fuzzy segments are shown in Figs. 2 and 3. We mean two groups of thick points indicating arrivals of rays with the identifiers +124 and +160. Closer views of these groups of points are shown in Fig. 12. The left (right) panel presents arrivals with the identifier +124 (+160). Thick solid lines in both panels show the unperturbed segments with the identifiers +124 (left panel) and +160 (right panel).

In order to derive quantitative characteristics of the fuzzy segment describing its spread and bias, we introduce the quantity  $\Delta\tau$  defined as follows. Consider a particular ray (perturbed) contributing to the fuzzy segment and denote its travel time by  $t_p$ . A travel time of an unperturbed ray with the same identifier

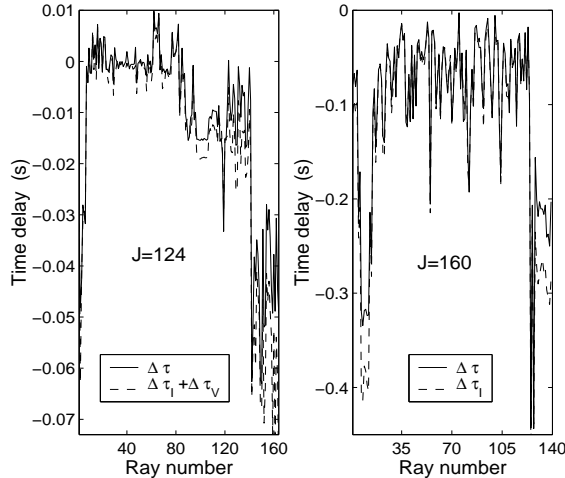


Figure 13: Time delays,  $\Delta\tau$ , defined by Eq. (115), for arrivals of rays with identifiers +124 (left panel) and +160 (right panel) at the range 3000 km. The solid lines represent results of the direct ray tracing, while the dashed lines are predictions made using Eq. (116). For rays with identifier +160 only the term  $\Delta\tau_I$  in Eq. (116) has been taken into account.

and the same arrival depth we denote by  $t_u$ . Then

$$\Delta\tau = t_p - t_u. \quad (115)$$

In words,  $\Delta\tau$  represents the distance along the  $t$ -axis between the given point of the fuzzy segment and the unperturbed segment with the same identifier. In the right panel of Fig. 12 the magnitude of  $\Delta\tau$  is shown for the earliest arrival. Note, that  $\Delta\tau$  is defined only for those rays forming the fuzzy segment whose arrival depths lie within a depth interval covered by the unperturbed segment. An approximate analytical expression for  $\Delta\tau$  is readily obtained from Eq. (107). Neglecting  $\Delta t_N$  which is identically zero for two rays with the same identifier, and  $\Delta t_G$  which is small in accordance to the remark made at the end of Sec. 6, we arrive at

$$\Delta\tau = \Delta\tau_I + \Delta\tau_V, \quad (116)$$

where

$$\Delta\tau_I = \frac{\bar{\omega}'}{2c_r} \int \Delta I^2 dr, \quad (117)$$

and

$$\Delta\tau_V = \frac{1}{c_r} \int \delta n(r, z(r)) dr. \quad (118)$$

First of all, check an accuracy of Eq. (116) at 3000 km range. This is done in Fig. 13 where we present travel time shifts  $\Delta\tau$  for arrivals shown in Fig. 12. In the perturbed waveguide there are 160 fan rays with the identifier +124 whose depths at 3000 km belong to the depth interval covered by the unperturbed fan rays, i.e. between upper and lower points of a solid curve in the left panel of Fig. 12. A solid line in the left panel of Fig. 13 connects exact values of  $\Delta\tau$  obtained by ray tracing, while a dashed line represents predictions provided by Eq. (116). Launch angles of perturbed rays with the identifier +124 belong to the interval  $(7^\circ, 9.5^\circ)$ . In Fig. 11 we see that the parameter  $\mu_3$  for such launch angles cannot be considered as small compared to unity, which means that both terms in Eq. (116) should be retained. In the right panel of Fig. 13 a similar plot is shown for 139 rays with the identifier +160. The prediction depicted by a dashed curve has been made by retaining only the term  $\Delta\tau_I$ , because launch angles of these rays are less than  $7^\circ$ . The parameter  $\mu_3$  for such launch angles is small (see Fig. 11) and the term  $\Delta\tau_V$  can be neglected. Figure 13 demonstrates that Eq. (116) provides a reasonable estimation for  $\Delta\tau$ .

Figure 12 exhibits a new phenomenon. The perturbation causes not only diffusion of the timefront segment but it also leads to some regular bias: rays with the given identifier in the perturbed waveguide arrive, on average, earlier than unperturbed rays with the same identifier. A similar bias is observed for every fuzzy segment. A qualitative explanation to this effect follows immediately from the fact that the term  $\Delta\tau_I$  in Eq. (116) usually dominates. This is true even of most steep rays although in this case the term  $\Delta\tau_V$  should be retained for obtaining an accurate prediction of  $\Delta\tau$ . The sign of  $\Delta\tau_I$  is determined by the sign of the derivative  $\bar{\omega}'$ . The latter is negative for rays propagating without reflection off the

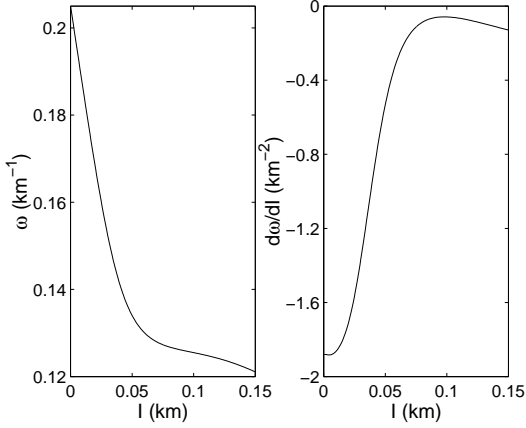


Figure 14: Left panel: Spatial frequency of ray trajectory oscillation,  $\omega$ , in the unperturbed waveguide as a function of the action variable,  $I$ . Right panel: The derivative of the spatial frequency  $\omega$  with respect to  $I$ .

surface and bottom, because in typical deep ocean waveguides the cycle length of the refracted ray grows with the launch angle. The spatial frequency  $\omega$  and its derivative with respect to  $I$  are shown in Fig. 14 for the model of unperturbed waveguide on which we rely in this paper.

Approximating  $\Delta\tau$  by  $\Delta\tau_I$  (i.e., practically, by  $\Delta t_I^{(2)}$ ), one can estimate a mean bias of the fuzzy segment,  $\langle \Delta\tau \rangle$ , by making use of Eq. (97) with  $\bar{I}$  equal to the mean action variable for the corresponding unperturbed segment. In Fig. 15 we compare this prediction (solid line) with “real” mean values of  $\Delta\tau$  (circles) evaluated for fuzzy segments formed by our fan rays with identifiers  $+J$  at ranges of 1500 km and 3000 km.

The rms time spread of the fuzzy segment can be estimated as

$$\begin{aligned} \sigma_{\Delta\tau} &= \sqrt{\langle (\Delta\tau - \langle \Delta\tau \rangle)^2 \rangle} \\ &= \sqrt{\langle \Delta\tau^2 \rangle - \langle \Delta\tau \rangle^2}. \end{aligned}$$

Approximating again  $\Delta\tau$  by  $\Delta\tau_I$  and making use of

Eq. (89) we get

$$\begin{aligned} \langle \Delta\tau^2 \rangle &= \left( \frac{\bar{\omega}'}{2c_r} \right)^2 \int_0^r \int_0^r d\rho_1 d\rho_2 \\ &\times [Q(\rho_1, \rho_1)Q(\rho_2, \rho_2) + 2Q^2(\rho_1, \rho_2)] = \left( \frac{\bar{\omega}'}{2c_r} \right)^2 \frac{\bar{B}_\xi^2 r^4}{20}. \end{aligned}$$

This yields

$$\sigma_{\Delta\tau} = \frac{|\bar{\omega}'| \bar{B}_\xi r^2}{c_r 6\sqrt{5}} = 0.9 |\langle \Delta\tau \rangle|, \quad (119)$$

i.e. the rms time spread is practically equal to its mean bias. In other words, Eq. (97) estimates not only the bias of the fuzzy segment but its time spread as well. In Fig. 16 we compare this prediction to “real” time spreads obtained in numerical simulation. Results presented in Figs. 15 and 16 demonstrate that even though predictions made with Eq. (97) have some systematic error for very flat rays (corresponding to large  $J$  in the lower panels of Figs. 15 and 16), these predictions are in reasonable agreement with numerical simulation and give the correct order of magnitude for both time spread and bias. In particular, we see that at 3000 km range, in accordance with Eq. (97), the bias and time spread become 4 times larger compared to their values at 1500 km.

Looking at Figs. 15 and 16 we see that the bias and time spread are especially small for segments formed by steep rays (small  $J$ ). On the right hand side of Eq. (97) there are two factors,  $\bar{B}_\xi$  and  $\bar{\omega}'$ , depending on  $\bar{I}$  and, hence, on the launch angle. Looking at Fig. 6 and at the right panel in Fig. 14 we conclude that the dependencies of  $\langle \Delta\tau \rangle$  and  $\sigma_{\Delta\tau}$  on the launch angle are mainly determined by the factor  $\bar{\omega}'$ .

### 7.2.2 Resolution of fuzzy segments in the perturbed timefront

In the upper panels of Figs. 2 and 3 it is clearly seen that unperturbed segments come in groups of four and each group consists of segments with the identifiers  $-(J-1)$ ,  $\pm J$ , and  $+(J-1)$ . The function

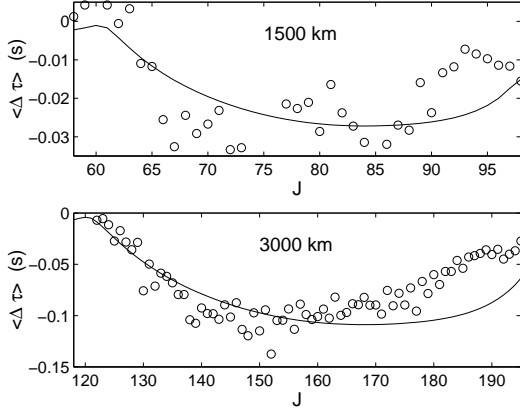


Figure 15: Mean bias of fuzzy segments due to inhomogeneities as a function of the ray identifier at ranges of 1500 km (upper panel) and 3000 km (lower panel). Each circle shows the bias averaged over a fuzzy segment, i.e. over a group of rays with the given identifier  $+J$ . The solid lines are predictions obtained using Eq. (97).

$\tau(\chi)$  defined by Eq. (114) predicts the time delay between two consecutive groups of four formed by rays with launch angles close to  $\chi$ . The difference in travel times of two neighboring segments can be roughly estimated as  $\tau/4$ . Estimating the width of the fuzzy segment as  $3\sigma_\tau$ , we introduce the parameter

$$R = \frac{12\sigma_\tau}{\tau} \simeq \frac{24\pi\bar{I}}{|\bar{\omega}'| \bar{B}_\xi r^2} \quad (120)$$

representing the ratio of the segment width to the time delay between neighboring segments. If  $R > 1$ , the fuzzy segment is resolved in the perturbed time-front while the segment with  $R < 1$  overlaps with neighboring segments. From the viewpoint of eigenrays, the condition  $R > 1$  ( $R < 1$ ) means that neighboring unperturbed eigenrays in the presence of perturbation split into nonoverlapping (overlapping) clusters.

In order to verify this prediction, consider the ray travel time,  $t$ , in the unperturbed waveguide as a function of the launch angle,  $\chi_s$ . For launch angles of the same sign the function  $t(\chi_s)$  is monotonic and

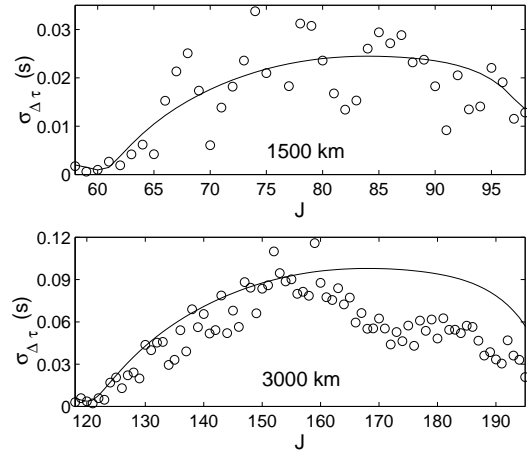


Figure 16: Width of a fuzzy segment as a function of the ray identifier at ranges of 1500 km (upper panel) and 3000 km (lower panel). Each circle shows the standard deviation of the time delay  $\tau$  obtained by averaging over the fuzzy segment, i.e. over a group of rays with the given identifier  $+J$ . The solid lines are predictions obtained using Eqs. (119) and (97).

the inverse function  $\chi_s(t)$  is unambiguous. Equation (120) defines the parameter  $R$  as a function of the launch angle  $\chi_s$ . Replacing  $\chi_s$  with  $\chi_s(t)$  we obtain the function  $R(t)$  that associates a value of parameter  $R$  with every segment of the unperturbed waveguide. If this value is greater than unity we expect that the fuzzy segment with the same identifier will be resolved. This statement is illustrated in Figs. 17 and 18. The functions  $R(t)$  at  $r = 1500$  km and  $r = 3000$  km evaluated for rays starting upward (for rays starting downward the results are practically the same) are plotted in the lower panels of Figs. 17 and 18. These functions are shown at time intervals where  $R(t)$  passes through 1. The corresponding portion of the perturbed timefronts from the upper panels of Figs. 2 and 3 are shown in the upper panels of Figs. 17 and 18. It is clearly seen that, indeed, the condition  $R = 1$  allows one to estimate the critical travel time which divides the perturbed timefront into parts consisting of resolved and unresolved fuzzy segments.

The fact that early arriving fuzzy segments formed by steep rays are well resolved is linked to the following two factors. First, the function  $\tau(\chi)$  grows with  $|\chi|$ . It means that the delay between two consecutive segments of the timefront formed by steep rays is larger than that for consecutive segments formed by flat rays. Second, the rms width of the fuzzy segment,  $\sigma_{\Delta\tau}$ , is especially small for steep rays (small  $J$ 's), as it is seen in Fig. 16.

### 7.2.3 Stability of fuzzy segments and Fermat's principle

Probably, the most surprising feature of the perturbed timefront is unexpectedly small widenings of timefront segments. In particular, in the upper panel of Fig. 16 we see that at 3000 km range the maximum rms widening of the fuzzy segment does not exceed 0.12 s. On the other hand, Fig. 4 demonstrates that a typical time spread for a cluster of rays with close launch angles is about 2 s, i.e. much larger. Loosely, we can state that the ray travel time dependence on the ray identifier is less chaotic and much more predictable than its dependence on the launch angle.

In order to interpret this phenomenon, we come

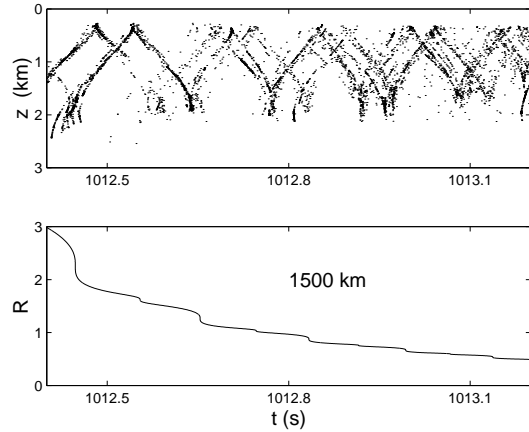


Figure 17: Upper panel: Fragment of the timefront at 1500 km range where transition from resolved to unresolved (overlapping) fuzzy segments is observed. Lower panel: Parameter  $R$  defined by Eq. (120) as a function of travel time. Theory predicts that resolved (unresolved) fuzzy segments are located to the left (right) of the travel time at which  $R$  passes through 1.

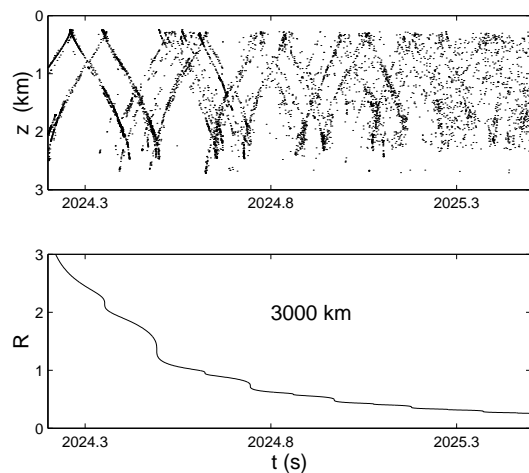


Figure 18: The same as in Fig. 17 for 3000 km range.

back to Eq. (116) and recall that the first term on the right side dominates. It means that the travel time shift between perturbed ( $P$ ) and unperturbed ( $U$ ) rays connecting the same points and having the same identifier can be approximately written as

$$\Delta\tau = \frac{1}{c_r}[S_0(P) - S_0(U)] \quad (121)$$

where  $S_0(P)$  and  $S_0(U)$  are the values of the functional  $S_0 = \int(pdz - H_0dr)$  evaluated over the trajectories of perturbed and unperturbed rays, respectively. According to Fermat's (Hamilton's) principle [9, 12, 14], the unperturbed ray provides a stationary path of the functional  $S_0$ . This fact explains the absence of the linear in  $\Delta I$  term in Eqs. (47) and Eq. (116). Since  $\Delta I$  is our small parameter, the absence of terms  $O(\Delta I)$  gives some qualitative interpretation of smallness of  $\Delta\tau$ . In this sense, the small time spread of clusters of rays with the same identifier can be interpreted as a consequence of Fermat's principle.

Note that the difference in travel times of rays with different identifiers ( $N \neq 0$ ) is defined mainly by the term  $\Delta t_N$  given by Eq. (46) which usually is significantly larger than  $\Delta t_I$ .

## 8 Action-angle variables in a waveguide with a range-dependent background sound-speed profile

An ocean-acoustic propagation model with the sound speed field being a superposition of a range-independent background and a weak range-dependent perturbation responsible for emergence of ray chaos may be too idealized. In this section we shortly outline how the results obtained in the preceding sections can be generalized to a more realistic model.

First, let us shortly discuss a method of introducing of the action-angle variables in the range-dependent waveguide [9] without dividing the Hamiltonian into a sum of an unperturbed term and a perturbation.

Define canonical transformations (14) and (15) at a current range  $r$  using Eqs. (18) and (19) evaluated for an auxiliary range-independent waveguide with the same cross-section that the real waveguide has at the range  $r$ . In this case the canonical transformation will be different at different ranges and Eqs. (14) and (15) translate to

$$I = I(p, z, r), \quad \theta = \theta(p, z, r) \quad (122)$$

and

$$z = z(I, \theta, r), \quad p = p(I, \theta, r). \quad (123)$$

The generating function  $G$  now becomes a function of not only  $I$  and  $z$ , but of  $r$ , as well. However,  $H = -\sqrt{n^2 - p^2}$  in the new variables is a function of  $I$  and  $r$ , but not  $\theta$  [9].

The Hamilton equations in the new variables preserve their canonical form

$$\frac{dI}{dr} = -\frac{\partial H_s}{\partial \theta}, \quad \frac{d\theta}{dr} = \frac{\partial H_s}{\partial I} \quad (124)$$

with the new Hamiltonian [9]

$$H_s(I, \theta, r) = H(I, r) + \Lambda(I, \theta, r), \quad (125)$$

where

$$\Lambda(I, \theta, r) = \left. \frac{\partial G(I, z, r)}{\partial r} \right|_{z=z(I, \theta, r)}. \quad (126)$$

The term  $\Lambda$  is small and can be neglected if range variations in the environment are adiabatic, i.e. if variations in the environment are small at the cycle of the ray trajectory. Then,  $dI/dr = 0$  and  $I$  remains constant along the ray trajectory, i.e. the action variable defined in this way does have a property of adiabatic invariance.

However, we suppose that this common approach is not convenient for description of the chaotic ray motion induced by random internal waves. The point is that if  $\Lambda$  is not negligible, then the connection between  $H$ ,  $\Lambda$  and  $\delta c$  becomes non-trivial, and it is difficult to divide Hamiltonian (125) into a sum of a smooth unperturbed term and a small perturbation.

But such a decomposition of the Hamiltonian is necessary for application of our perturbation theory.

A more appropriate approach can be developed if the sound speed field is a sum of a **smooth** range-dependent sound speed,  $c_0(r, z)$ , and a weak perturbation,  $\delta c(r, z)$ , i.e.

$$c(r, z) = c_0(r, z) + \delta c(r, z). \quad (127)$$

Instead of the range-independent unperturbed waveguide considered in the preceding sections, now we have an adiabatic one. Then, it is convenient to introduce the action-angle variables at every range  $r$  using an auxiliary range-independent waveguide with the cross-section coinciding with that of the unperturbed waveguide. This yields the new Hamiltonian in the form

$$H_s = H_0(I, r) + V(I, \theta, r), \quad (128)$$

where  $V(I, \theta, r)$  is the perturbation defined in Eq. (23) with the unperturbed refractive index  $n_0$  now depending not only on  $z$  but on  $r$ , as well. Then the Hamilton equations have the same form as Eqs. (28) and (29) in Sec. 3.2, although the angular frequency  $\omega$  now depends on  $r$ ,  $\omega(I, r) = \partial H_0(I, r) / \partial I$ . All expressions for differences in ray travel times of perturbed and unperturbed rays derived in Sec. 4 remain valid for this more realistic model.

## 9 Summary and conclusion

In this paper we have derived the approximate analytical approach for description of ray travel times and other parameters of the ray structure in deep ocean environment. Our results remain valid at ranges up to, at least, a few thousand km. The approach is based on the assumptions that (i) the perturbation giving rise to the chaotic ray motion is small and (ii) even at long ranges rms variations of the action variable are small compared to the characteristic scale of function  $\omega(I)$ . The dimensionless small parameters in the problem are given by Eqs. (103)–(105).

The exact expression for the difference in travel times of perturbed and unperturbed rays,  $\Delta t$ , determined by Eqs. (45) – (50) has been significantly simplified by expanding it in a power series in  $\Delta I$  and neglecting small terms. The smallness of fluctuations of the action variable has also been used to simplify the stochastic ray (Hamilton) equations. It has been shown that the fluctuating components of the action and angle variables can be idealized as a Wiener process, and an integral of the Wiener process, respectively. This result, which allows one to evaluate (approximately) practically any statistical characteristic of the ray trajectory, in the present paper has been combined with an approximate formula for  $\Delta t$  and applied for investigation of range variations of ray travel times.

Our primary concern has been with the range variations of the timefront representing ray arrivals in the time-depth plane. The unperturbed timefront consists of segments of smooth curves. Each segment is formed by rays with the same identifier. In the presence of perturbation segments become fuzzy: arrivals with the given identifier form a set of points randomly scattered around the unperturbed segment. The time spread of these points turns out to be unexpectedly small. It is much less than a time spread of arrivals with launch angles within a narrow angular interval corresponding to launch angles of rays forming an unperturbed segment. The most apparent manifestation of this phenomenon is a surprising stability of early portions of the timefront formed by steep rays [3, 4, 5, 6].

Our approach provides a quantitative description of fuzzy segments. It gives estimations of their widths and biases. Using these estimations, it follows that the sign of the bias is determined by the sign of  $d\omega/dI$ , the derivative of the spatial frequency of ray oscillation in the unperturbed waveguide with respect to the action variable. In typical deep ocean waveguides  $d\omega/dI < 0$  for all refracted rays, which means that fuzzy segments have negative bias, i.e. perturbed rays, on average, arrive earlier compared to unperturbed rays with the same identifier. It has been shown that the surprising stability of fuzzy segments with respect to the perturbation is related to the Fermat's (Hamilton's) principle.

The estimations derived for the timefront segments can be applied to study characteristics of chaotic eigenrays. In Ref. [22] (see also Ref. [23]) it has been discovered numerically, that in the presence of a weak perturbation the unperturbed eigenray splits into a cluster of new eigenrays with close arrival times. The time spread of such a cluster can be estimated as a time spread of the corresponding fuzzy segment at the corresponding depth. So, our criterion of nonoverlapping of neighboring segments (120) provides the criterion of resolution for clusters of eigenrays.

It should be emphasized that results of the present work have been obtained for the perturbation induced by internal waves. Their generalization to the case of other inhomogeneities, e.g. the mesoscale inhomogeneities, requires a further investigation.

## Acknowledgment

I thank Prof. G. Zaslavsky for benefit of our discussions on problems of quantum and wave chaos. I am grateful to Dr. I.P. Smirnov whose ray code has been used for numerical simulations. The work was supported by the U.S. Navy Grant N00014-97-1-0426 and by the Grants 00-02-17409 and 01-05-64394 from the Russian Foundation for Basic Research.

## A Appendix. Evaluation of action and angle variables using a ray code

Explicit analytical relations connecting the position-momentum and action-angle variables can be derived only for a few simple refraction index profiles  $n_0(z)$  [10, 13]. In underwater acoustics the researcher is usually forced to deal with refraction index profiles defined by spline approximations of data measured at discrete depths. In this case ray trajectories are computed using standard ray codes which allow one evaluate such parameters of the ray as the coordinate, momentum, and travel time [14]. Fortunately, the same codes can be applied for evaluation of the action and angle variables. It will be a simpler and

more convenient procedure compared to the direct application of Eqs. (18) and (19).

As it has been pointed out in Secs. 3.2 and 8 the transformation from the position-momentum to the action-angle variables is **always** defined using an auxiliary range-independent waveguide. So what we need for establishing relations between the two types of variables in any waveguide, is a code for computing the ray path in the range-independent waveguide.

The action variable for the given trajectory can be easily found by evaluating the integral

$$I = \frac{1}{2\pi} \int_0^D \frac{p^2(r)}{\sqrt{n_0^2(z(r)) - p^2(r)}} dr \quad (129)$$

where the functions  $z(r)$  and  $p(r)$  are the coordinate and the momentum, respectively, as functions of range, and  $D$  is the cycle length. Here we have applied Eqs. (11) and (6). Computing ray paths corresponding to different values of the Hamiltonian (9) and using a spline approximation we find functions  $H_0(I)$ ,  $I(H_0)$ , and  $\omega(I) = 2\pi/D(I)$ .

Then the transformation from  $(p, z)$  to  $(I, \theta)$  is performed as follows. Substituting the given  $p$  and  $z$  into Eq. (9) yields  $H_0$ . Then, making use of the function  $I(H_0)$  we get the action variable,  $I$ . In order to find the angle variable,  $\theta$ , consider a ray trajectory with  $H_0$  determined by the given  $p$  and  $z$ , which begins at its upper turning point, i.e. at  $z(0) = z_{\min}$  (recall that we are using  $z$ -axis directed downward). According to Eq. (21)

$$r = \theta/\omega(I). \quad (130)$$

It means that a minimum range,  $r$ , at which the trajectory has the coordinate and momentum equal to the given  $p$  and  $z$ , respectively, defines the desired angle variable,  $\theta$ .

In order to use Hamilton equations (28) and (29) in practice we need a numerical procedure which allows one to express an arbitrary function  $F(p, z)$  as a function of  $I$  and  $\theta$ , by replacing the arguments  $p$  and  $z$  with  $p(I, \theta)$  and  $z(I, \theta)$ . In other words, we need a function  $\Phi(I, \theta) \equiv F(p(I, \theta), z(I, \theta))$ . In principle, it can be found by a direct substitution. However, there exists a following more convenient procedure.

Since both  $p(I, \theta)$  and  $z(I, \theta)$  are periodic in  $\theta$  with the period  $2\pi$ , the function  $\Phi(I, \theta)$  is also periodic and it can be represented as a Fourier series

$$\Phi(I, \theta) = \sum_{n=0}^{\infty} A_n(I) \cos n\theta + \sum_{n=1}^{\infty} B_n(I) \sin n\theta, \quad (131)$$

where

$$\begin{aligned} \begin{pmatrix} A_n(I) \\ B_n(I) \end{pmatrix} &= M_n \\ \times \int_0^{2\pi} d\theta \Phi(I, \theta) \begin{pmatrix} \cos n\theta \\ \sin n\theta \end{pmatrix}, & \quad (132) \\ M_n &= \begin{cases} 1/2\pi, & n = 0 \\ 1/\pi, & n > 0 \end{cases}. \end{aligned}$$

Using relation (130) we can express the above integrals via the integrals over the ray trajectory computed with the ray code. This yields

$$\begin{aligned} \begin{pmatrix} A_n(I) \\ B_n(I) \end{pmatrix} &= M_n \omega(I) \\ \times \int_0^{2\pi} dr' F(p(r'), z(r')) \begin{pmatrix} \cos n\omega(I)r' \\ \sin n\omega(I)r' \end{pmatrix}. & \quad (133) \end{aligned}$$

If the function  $F$  depends not only on  $p$  and  $z$ , but on range  $r$ , as well, then the function  $\Phi$  and the coefficients  $A_n$  and  $B_n$  acquire an additional argument  $r$ . In Eq. (133) this argument should be considered as a constant, i.e. there should be no integration over this argument.

Note that functions  $p(r)$  and  $z(r)$  in Eq. (133) which define a trajectory in the auxiliary waveguide may be quite different from range dependencies of coordinates and momenta for “real” ray trajectories satisfying Hamilton equations (6) and (7).

## References

- [1] S.M. Flatte, R. Dashen, W.M. Munk, K.M. Watson, and F. Zakhariassen. *Sound transmission through a fluctuating ocean*. Cambridge U.P., London, 1979.
- [2] J. A. Colosi and M.G. Brown. Efficient numerical simulation of stochastic internal-wave-induced sound-speed perturbation field. *J. Acoust. Soc. Am.*, 103:2232–2235, 1998.
- [3] M.G. Brown and J. Viechnicki. Stochastic ray theory for long-range sound propagation in deep ocean environment. *J. Acoust. Soc. Am.*, 104:2090–2104, 1998.
- [4] J. Simmen, S.M. Flatte, and G.-Y. Wan. Wavefront folding, chaos, and diffraction for sound propagation through ocean internal waves. *J. Acoust. Soc. Am.*, 102:239–255, 1997.
- [5] P. F. Worcester, B. D. Cornuelle, M. A. Dzieciuch, W. H. Munk, M. Howe, A. Mercer, R. C. Spindel, J. A. Colosi, Metzger, T. Birdsall, and A. B. Baggeroer. A test of basin-scale acoustic thermometry using a large-aperture vertical array at 3250-km range in the eastern north pacific ocean. *J. Acoust. Soc. Am.*, 105:3185–3201, 1999.
- [6] J. A. Colosi, E. K. Scheer, S. M. Flatte, B. D. Cornuelle, M. A. Dzieciuch, W. H. Munk, P. F. Worcester, B. M. Howe, J. A. Mercer, R. C. Spindel, K. Metzger, T. Birdsall, and A. B. Baggeroer. Comparisons of measured and predicted acoustic fluctuations for a 3250-km propagation experiment in the eastern north pacific ocean. *J. Acoust. Soc. Am.*, 105:3202–3218, 1999.
- [7] W. Munk and C. Wunsch. Ocean acoustic tomography: A scheme for large scale monitoring. *Deep-Sea Res.*, 26:123–161, 1979.
- [8] J. Spiesberger and K. Metzger. Basin-scale tomography: a new tool for studying weather and climate. *J. Geophys. Res.*, 96:4869–4889, 1991.
- [9] L.D. Landau and E.M. Lifshits. *Mechanics*. Nauka, Moscow, 1973.
- [10] S.S. Abdullaev and G.M. Zaslavsky. Classical nonlinear dynamics and chaos of rays in wave propagation problems in inhomogeneous media. *Usp. Fiz. Nauk*, 161(8):1–43, 1991.

- [11] J.L. Spiesberger. Ocean acoustic tomography: Travel time biases. *J. Acoust. Soc. Am.*, 77:83–100, 1985.
- [12] M. Born and E. Wolf. *Principles of optics*. Pergamon Press, Oxford, 1968.
- [13] S.S. Abdullaev. *Chaos and dynamics of rays in waveguide media*. Gordon and Breach science publishers, New York, g. zaslavsky edition, 1993.
- [14] F.B. Jensen, W.A. Kuperman, M.B. Porter, and H. Schmidt. *Computational Ocean Acoustics*. AIP, Woodbury, New York, 1994.
- [15] L.M. Brekhovskikh and Yu. Lysanov. *Fundamentals of Ocean Acoustics*. Springer-Verlag, Berlin, 1991.
- [16] V.I. Tikhonov and M.A. Mironov. *Markov processes*. Sovetskoe Radio, Moscow, 1977.
- [17] S.M. Rytov. *Introduction to statistical radio-physics. Part I*. Nauka, Moscow, 1976.
- [18] S.N. Gurbatov, A.N. Malakhov, and A.I. Saichev. *Nonlinear random waves and turbulence in nondispersive media: waves, rays, particles*. Manchester University Press, Manchester, 1991.
- [19] A.L. Virovlyanskii. Travel times of acoustic pulses in the ocean. *Sov. Phys. Acoust.*, 31:399–401, 1985.
- [20] W.Munk and C.Wunsch. Ocean acoustic tomography: rays and modes. *Rev. Geophys. and Space. Phys.*, 21:1–37, 1983.
- [21] A.L. Virovlyansky. On general properties of ray arrival sequences in oceanic acoustic waveguides. *J. Acoust. Soc. Am.*, 97:3180–3183, 1995.
- [22] F.D. Tappert and X. Tang. Ray chaos and eigen-rays. *J. Acoust. Soc. Am.*, 99:185–195, 1996.
- [23] J.L. Spiesberger and F.D. Tappert. Kaneohe acoustic thermometer further validated with rays over 3700 km and the demise of the idea of axially trapped energywavefront folding, chaos, and diffraction for sound propagation through ocean internal waves. *J. Acoust. Soc. Am.*, 99:173–184, 1996.